Double Helix of Opposite Charges to Form Channels with Unique CO_2 Selectivity and Dynamics

Guolong Xing,[a,b] Irene Bassanetti,[b] Silvia Bracco,[b] Charl Bezuinedhout,[b] Mattia Negroni,[b] Teng Ben,[a,] Piero Sozzani[b,*] and Angiolina Comotti[b,*]*

[a] Department of Chemistry, Jilin University, 130012 Changchun, China

[b] Department of Materials Science, University of Milano-Bicocca, Via R. Cozzi 55, 20125 Milan, Italy.

Email: piero.sozzani@unimib.it

Table of Contents

1. Methods

Synthesis of CPOS-5. The monomers 4,4',4'',4'''-methanetetrabenzenesulfonic acid (H_4TBS), terephtalimidamide hydrochloride (DAB·HCl) were synthesized according the previously published literature.[1] All other reagents and solvents are commercially available and were used as received. 4,4',4'',4'''-Methanetetrayltetrabenzenesulfonic acid (H_4TBS, 20.5 mg, 0.024 mmol), was dissolved in 0.1 mL of aqueous NaOH1M followed by dissolving in 0.9 mL distilled water and 2.0 mL tetrahydrofuran (THF) in a vial. Then terephthalimidamide hydrochloride (DAB·HCl, 11.5 mg, 0.096 mmol) was dissolved in 1.00 mL distilled water and 2.00 ml THF in another vial. The vials were swirled mildly for complete mixing of the aforesaid solutions. After this, the solution was added drop wise to 4,4',4'',4'''-methanetetrabenzenesulfonic acid acid solution. The sealed vial was left undisturbed at room temperature overnight. The needle-like light yellow crystals obtained, were filtrated and then washed with a solution of water and THF (1:2 ratio by volume), yielding the organosulfonate-amidinium compound CPOS-5. CPOS-5 was activated by thermal treatment under vacuum overnight at 150°C.

NMR spectroscopy. ^{1}H-NMR and ^{13}C{^{1}H}-NMR spectra were recorded on 400 MHz Bruker instruments. Chemical shifts are reported in ppm relative to the solvent residual peak of $(CD_3)_2SO$ (δ^{1}H 2.50, δ^{13}C 39.5).

Infrared Spectroscopy (IR). To carry out the Fourier transform infrared spectroscopy (FTIR), a mixture of the sample and KBr (Aldrich) was prepared and pressed to form pellets. Then the FTIR spectra were recorded from the pellets using a SHIMADZU IRAFFINITY-1 FTIR spectrophotometer (4000-400 cm^{-1} interval).

Thermal Gravimetric analysis (TGA). The thermogravimetric analysis (TGA) of the samples was carried out by loading the samples in an alumina pan using a SHIMADZU DTG-60 thermal analyzer at the heating rate of 10 °C min-1 to 900 °C under the dried air atmosphere with an air flow rate of 30 mL min^{-1}.

Single Crystal X-ray Crystallography (SCXRD). The crystal measurement of CPOS-5 at 100 K was performed at Elettra Syncrotron (Trieste, Italy) on beamline XRD1 under cold nitrogen flux. The source used for the analysis was a NdBFe Multipole Wiggler (Hybrid linear), 4.27 KeV with a power of 8.6 kW, a source size FWHM of 2.0 x 0.37 mm (0.7 x 0.2 mm FWHM beam size at sample) and photon flux 1012-1013 ph/sec. Crystals were mounted with cryoloops (0.05-0.3 mm), prior a flash freezing at 100 K. Diffraction data were indexed, integrated, and scaled using CrysAlis software. Data collection of CPOS-5 at 273 K was performed on a Bruker D8-Venture diffractometer with a Turbo X-ray Source Mo K_α radiation (λ = 0.71073 Å). The intensity data were integrated from several series of exposure frames covering the sphere of reciprocal space. The data frames were collected using the program APEX2 and processed using the program SAINT routine in APEX2 (Bruker-AXS (2014). *APEX2.* Version 2014.11-0. Madison, Wisconsin, USA). Both structures were then solved by direct methods using SHELXS[2] and refined by full-matrix least-squares on all F2 using SHELXL implemented in Olex2.[3] For all the structures, anisotropic displacement parameters were refined except for hydrogen atoms. The OLEX2 solvent mask was used to correct for the unmodeled water molecules of the 273 K crystal structure.

Powder X-ray Diffraction (PXRD). Powder X-ray diffraction (PXRD) measurements were accomplished with a PANalytical B.V. Empyrean powder diffractometer using Cu-Kα radiation, 40 kV, 40 mA over a range of 2θ = 4.0-40.0 with a step size of 0.02° and 2s per step. Indexing and Rietveld refinement were performed using the TOPAS-Academic-64 V6 software package.[4] The initial input structure used for the PXRD refinement was generated using DFT calculations. The DFT optimizations had the unit-cell restrained to the PXRD indexed cell parameters while all the molecules could be optimized. Optimizations were performed using the GGA PBE functional with Grimme's DFT-D dispersion correction, thresholds for geometry optimization and SCF convergence were chosen as 2×10^{-6} eV. The unit-cell parameters where kept fix while all the atoms where allowed to optimize using the symmetry of the system ($I4_1$). The hydrogen atoms of the DFT optimized structure were normalized to neutron diffraction distances using the normalized option in the Mercury V 3.9.[5] The unit-cell parameters were kept fix throughout the refinement process. The refined

structure was optimized using DFT and the hydrogen atoms normalized followed by another Rietveld refinement step. This protocol was repeated until there was reasonable agreement between the DFT stable structure and the PXRD Rietveld refined structure. The background was fitted and refined using a Chebyshev polynomial with 10 coefficients in the range of the PXRD trace from 5° to 38° 2theta and the application of baseline shift refinement. Other corrections include: Specimen Displacement, Divergence Sample Length, Absorption with Sample Thickness Shape Intensityand Specimen Tilt. The peaks were fitted using a modified Thompson-Cox-Hastings pseudo-Voigt "TCHZ" profile. Preferred orientation was considered using a combination of March Dollase (1 0 0, 0 1 0, 0 0 1, 1 1 0, 0 1 1, 1 0 1) and a sixth order Spherical Harmonics refinement.

Gas Adsorption measurements. CO_2, CH_4 and N_2 sorption experiments at 298 K, 273 K and 195 K up to 1 bar were collected using a Micromeritics ASAP 2020 surface area and pore size analyzer. Gas sorption isotherms at 298 K and 273 K and up to 10 bar were collected on Micromeritics ASAP 2050. Before sorption analysis, the samples were evacuated at 150 °C for overnight using a turbo molecular vacuum pump. Specific surface areas were calculated from CO_2 adsorption data by multipoint BET analysis. Pore size distributions were calculated from the CO_2 adsorption isotherms using non-local density functional theory (NLDFT) method. Ultra-high-purity grade N_2 (99.999%), CO_2 (99.999%) and CH_4 gases (99.99%) were used for all adsorption measurements. Helium (99.999%) was used to measure the free space. Gas isotherms at 273 K and 298 K were measured using a cryostat Julabo F12-ED to keep the temperatures stable. The isosteric heat of adsorption Q_{st} values were determined by applying the Vant'Hoff equation. The selectivities of CO_2/N_2 binary mixtures were determined from the single-component isotherms using the Ideal Adsorbed Solution Theory (IAST) and a CO_2/N_2 ratio of 15:85 (mol:mol). At room temperature the CO_2/N_2 selectivity was also calculated from the ratio of Henry's constants.

Solid State NMR (SS-NMR). Solid-state NMR spectra were run at 75.5 MHz for ^{13}C on a Bruker Avance 300 instrument operating at a static field of 7.04 T equipped with high-power amplifiers (1 kW) and a 4 mm

double resonance MAS probe. $^{13}C\{^{1}H\}$ ramped-amplitude cross polarization (CP) MAS experiments were performed at room temperature at a spinning speed of 12.5 kHz, using a contact time of 0.05, 2 and 5 ms. The 90° pulse used for proton was 2.9 μs. ^{13}C Single-pulse excitation (SPE) experiments were run using a 90° pulse of 4.6 μs. Crystalline polyethylene was taken as an external reference at 32.8 ppm from TMS. ^{13}C-enriched CO_2 (isotopic purity of 99%) was used. A MAS NMR 4mm rotor containing empty CPOS-5 (47.8 mg) has been treated at 373 K under vacuum overnight. We used an home-made apparatus that allows to seal the rotor, after equilibration under controlled gas temperature and pressure. The CO_2 adsorption has been performed at a constant pressure of 550 torr at 210 K for 2 h. The CO_2 amount in the rotor was weighted as 3.66 mg. The partitioning between CO_2 in the gas phase and CO_2 adsorbed in the sample was evaluated quantitatively by the deconvolution of the ^{13}C NMR spectra. At 298 K the amount of adsorbed $^{13}CO_2$ corresponds to 5.9 CO_2 molecules per unit cell.

The CPOS-5 sample with adsorbed $^{13}CO_2$ was characterized under both magic angle spinning (MAS) and static conditions. ^{13}C SPE-MAS NMR spectrum of CPOS-5 in the presence of $^{13}CO_2$ has been collected at 298 K at a spinning speed of 10 kHz with a recycle delay of 20 s. The $^{13}C\{^{1}H\}$ CP MAS experiments of CPOS-5 with adsorbed $^{13}CO_2$ were performed at 5 ms and a spinning speed of 8 kHz at 296 and 266 K. We observed that the CP efficiency was retained even in the upper limit of temperatures. ^{13}C SPE static NMR spectra were performed at variable temperature in the range 295 K - 215 K with a recycle delay of 15 s.

Phase-modulated Lee−Goldburg (PMLG) heteronuclear ^{1}H-^{13}C correlation (HETCOR) experiments coupled with fast magic angle spinning allowed the recording of the 2D NMR spectra with a high resolution in both hydrogen and carbon dimensions. Narrow hydrogen resonances, with line widths of the order of 1-2 ppm, were obtained with homonuclear decoupling during t_1; this resolution permitted a sufficiently accurate determination of the proton species in the system. The 2D ^{1}H - ^{13}C PMLG HETCOR spectra were run with an LG period of 18.9 μs. The efficient transfer of magnetization to the carbon nuclei was performed by applying the RAMP-CP sequence. Quadrature detection in t_1 was achieved by the time proportional phase increments method (TPPI). The carbon signals were acquired during t_2 under proton decoupling by applying the two-pulse phase modulation scheme (TPPM).

The 2D ^{1}H-^{13}C PMLG HETCOR NMR spectra of empty CPOS-5 were conducted at 298 K under magic-angle spinning (MAS) conditions at 12.5 kHz with cross polarization times of 0.05 ms, 0.25 ms and 2 ms, and at 266 K with a spinning speed of 8 kHz and 5 ms of contact time. The 2D NMR spectra of CPOS-5 sample with adsorbed $^{13}CO_2$ were collected at 298 K at 10 kHz with contact times of 0.5 and 1 ms whilst at 266 K at 8 kHz with a contact time of 5 ms.

Computational Details. Atomic coordinates were imported from the refined crystal structures. The hydrogen atoms in the frameworks were optimized as part of a periodic system. The optimizations and single point energy calculations were performed using the GGA PBE functional with Grimme's DFT-D dispersion correction, and thresholds for geometry optimization and SCF convergence were chosen as 2×10^{-6} eV (optimizations) and 1×10^{-6} eV (single point). The convergence tolerances for the geometry optimizations were set to 2×10^{-5} eV/atom (Energy), 0.05 eV/Å (max force) and 0.002 Å (max displacement). The Milliken charges were calculated at the end of the SCF cycle. These atomic charges were used in the Molecular Mechanics (MM) and Molecular Dynamics (MD) calculations. The electrostatic potentials and electron density data were calculated as a single point energy calculation. An all-electron core treatment was used in conjunction with the DNP basis-set and the grid size for the imported electrostatic potential was set to 0.1 Å. The electron density data obtained were used to construct the three-dimensional 0.01 $e^{-}/Å^{3}$ electron density contours of the CO_2 molecules. The molecular electrostatic potential calculated for the host was then mapped onto the electron density contours of the CO_2 molecules.

A Quench Dynamics protocol was used to perform a configurational search for the possible guest positions and arrangements. DFT optimizations were performed to obtain the energies of the most probable guest arrangements. Single point energies were used to determine the interaction energies between the host and the guest.

The energy barrier for the diffusion of a CO_2 molecule was performed by a transition state (TS) search. The host molecules for both the minimum and transition state were optimized with the fractional coordinates of the CO_2 molecules fixed. This was followed by a single point calculation using a SCF convergence of 5×10^{-7} eV

and “Density Mixing” electronic minimizer. The energy barrier was then calculated by the difference between the energy of minimum and the transition state.

Regarding the CO_2 loading simulations, a supercell of CPOS-5 was constructed by considering 4 unit-cells along the *c*-axis. The supercell was loaded from 1 molecule per unit cell (MPU) (1 MPU ≡ 4 molecules per supercell) to 12 MPU with an increment of 1 MPU. For each loading step Molecular Dynamics (MD) simulations were performed, followed by full unit-cell Molecular Mechanics (MM) optimizations on 300 frames (structures) extracted from the MD simulations. The unit-cell parameters and CO_2 inclination angles (θ) were extracted from each frame and consolidated to evaluate the data statistically. The unit-cell parameters were averaged across the data set for each loading step (from 1 -12 MPU). The CO_2 inclination angles were converted to a distribution with a bin size of 0.1°, normalized to a sum of 1 and then smoothed using an FFT filter with a window size of 10 (total data points are between 2000 - 4000). On the subsequent processed plot, Gaussian peak profile fitting was performed to deconvolute the angle distributions into quantitative regimes. Each peak position was weighted by its peak area and then added together to yield the weighted average CO_2 angle (for each loading increment or step).

2. ^{1}H and ^{13}C liquid NMR

^{1}H-NMR and $^{13}C\{^{1}H\}$-NMR spectra were recorded on 400 MHz Bruker instruments. Chemical shifts are reported in ppm relative to the solvent residual peak of $(CD_3)_2SO$ ($\delta^{1}H$ 2.50, $\delta^{13}C$ 39.5).

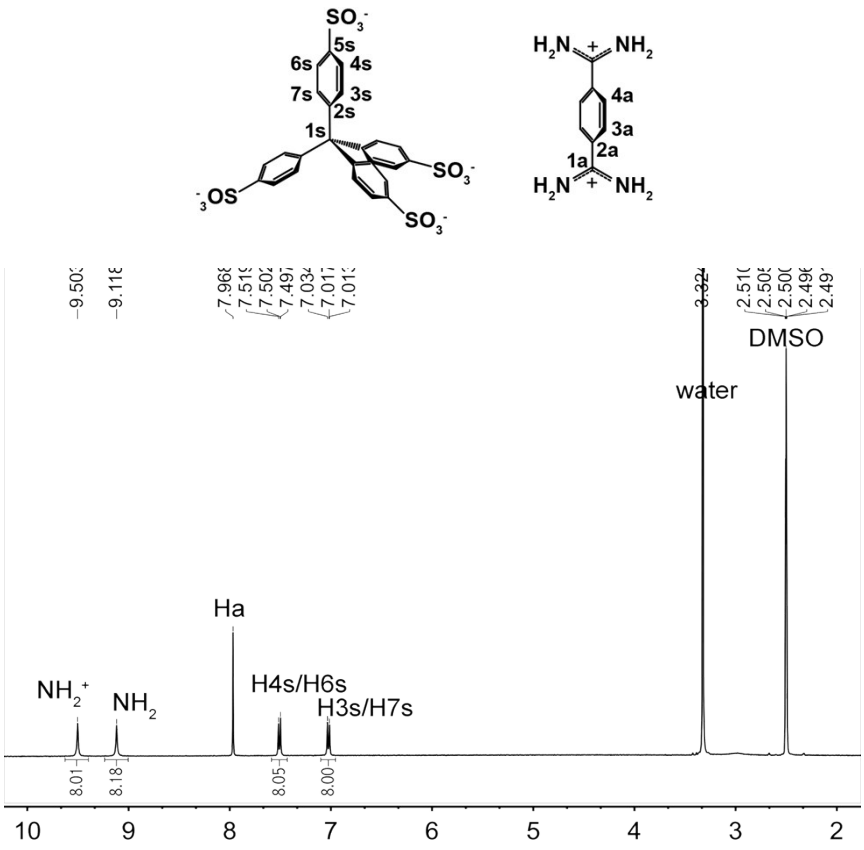

Figure S1. ^{1}H-NMR spectra of CPOS-5 in DMSO at room temperature. ^{1}H-NMR (400 MHz, DMSO): δ 7.02 (d, 8H, J= 8Hz, CH-$C_{aromSO3}$), 7.51 (d, 8H, J= 8Hz, CH-$SO_{3aromSO3}$), 7.97 (s, 8H, $CH_{terephtal}$), 9.12 (s, 8H, NH_2), 9.50 (s, 8H, $N^{+}H_2$) ppm.

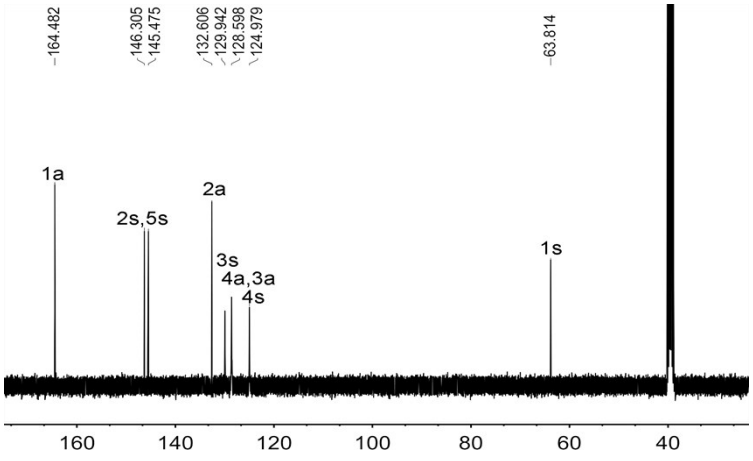

Figure S2. ^{13}C-NMR of CPOS-5 in DMSO at room temperature. ^{13}C-NMR (400 MHz, DMSO): δ 63.81, 124.98, 128.60, 129.94, 132.61, 145.47, 146.30, 164.48 ppm.

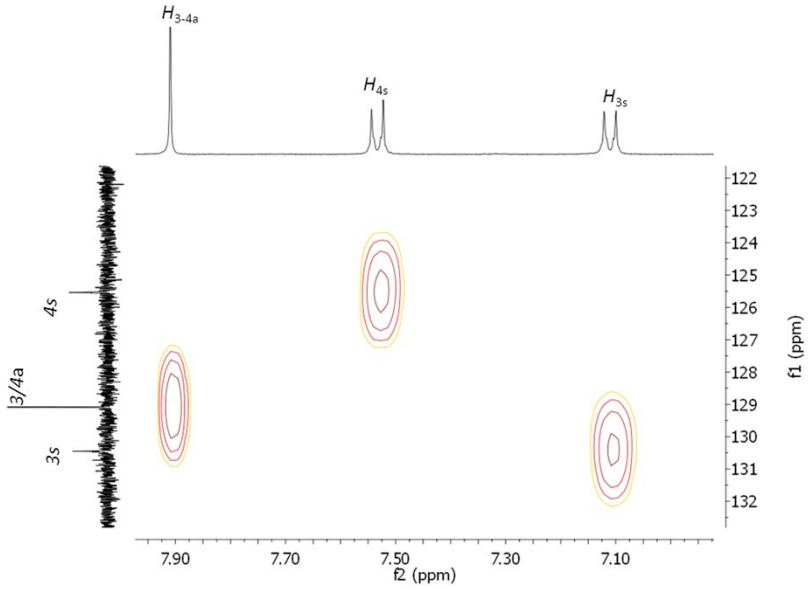

Figure S3. ^{1}H-^{13}C HSQC NMR spectra of CPOS-5 in DMSO at room temperature.

3. Infrared Spectroscopy FTIR and Thermogravimetric Analysis TGA

To carry out the Fourier transform infrared spectroscopy (FTIR), a mixture of the sample and KBr (Aldrich) was prepared and pressed to form pellets. Then the FTIR spectra were recorded from the pellets using a SHIMADZU IRAFFINITY-1 FTIR spectrophotometer (4000-400 cm^{-1} interval).

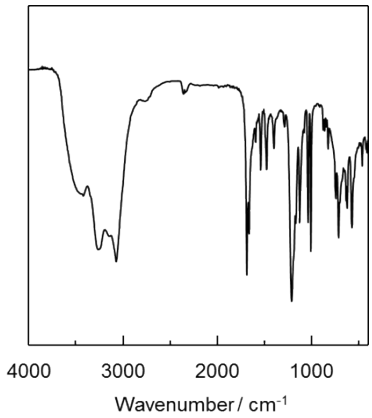

Figure S4. FT-IR spectra of CPOS-5. (KBr): ν/cm^{-1} 3420 (m), 3262(s), 3142(m), 3071(s), 1688(s), 1664(m), 1595(w), 1541(m), 1479(m), 1402(m), 1288(w), 1213(s), 1169(m), 1128(m), 1080(w), 1038(m), 1009(s), 880(w), 864(w), 845(w), 826(w), 743(m), 716(m), 637(m), 623(m), 573(w), 465(w)

The thermogravimetric analysis (TGA) of the samples was carried out by loading the samples in an alumina pan using a SHIMADZU DTG-60 thermal analyzer at the heating rate of 10 °C min-1 to 900 °C under the dried air atmosphere with an air flow rate of 30 mL min^{-1}.

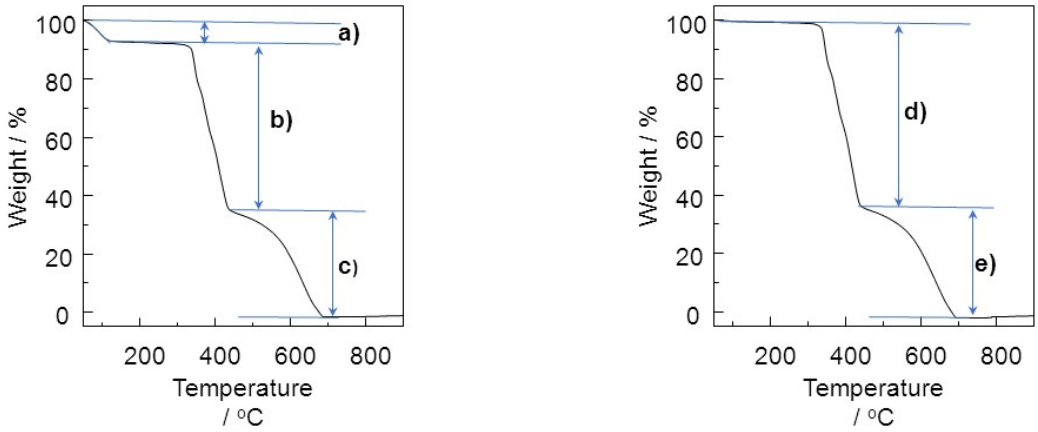

Figure S5. TGA plot of CPOS-5 (left side) under air condition: a) 7.5% weight loss attributable to guests (water/THF) removal; b) 56.9% weight loss attributable to organic salt decomposition; c) 37.3% weight loss attributable to final degradation. TGA plot of empty CPOS-5 (right side) under air condition: d) 63.7% weight loss attributable to organic salt decomposition; e) 38.2% weight loss attributable to final degradation.

4. X-ray diffraction data from single crystal (SC-XRD) and powder crystalline compounds (PXRD)

Table S1. Crystallographic data from the Single Crystal X-ray diffraction experiments.

Identification code	**CPOS-5_100 K**	**CPOS-5_273 K**
Empirical formula	$C_{164}H_{224}N_{32}O_{80}S_{16}$	$C_{164}H_{160}N_{32}O_{48}S_{16}$
Formula weight	4436.70	3860.19
Temperature/K	100	273.15
Crystal system	tetragonal	tetragonal
Space group	$I4_1/a$	$I4_1/a$
a/Å	25.7276(5)	25.1179(7)
b/Å	25.7276(5)	25.1179(7)
c/Å	7.7202(3)	7.6702(5)
α/°	90	90
β/°	90	90
γ/°	90	90
Volume/Å^3	5110.1(3)	4839.2(4)
Z	16	16
ρ_{calc}g/cm^3	1.442	1.325
μ/mm^{-1}	0.260	0.262
F(000)	2328.0	2008.0
Crystal size/mm^3	0.733 × 0.023 × 0.022	0.733 × 0.023 × 0.022
Radiation	synchrotron (λ = 0.70000)	MoK_α (λ = 0.71073)
2Θ range for data collection/°	4.41 to 51.878	4.586 to 50.038
Index ranges	$-32 \le h \le 32$, $-32 \le k \le 32$, $-9 \le l \le 9$	$-26 \le h \le 28$, $-9 \le k \le 29$, $-8 \le l \le 9$
Reflections collected	24962	6929
Independent reflections	2609 [R_{int}= 0.1164, R_{sigma}= 0.0343]	2116 [R_{int}= 0.0638, R_{sigma}= 0.0837]
Data/restraints/parameters	2609/0/177	2116/6/158
Goodness-of-fit on F^2	1.083	1.153
Final R indexes [I>=2σ (I)]	R_1= 0.0486, wR_2= 0.1401	R_1= 0.0936, wR_2= 0.2728
Final R indexes [all data]	R_1= 0.0503, wR_2= 0.1429	R_1= 0.1280, wR_2= 0.3100
Largest diff. peak/hole / e Å^{-3}	0.36/-0.57	0.55/-0.92

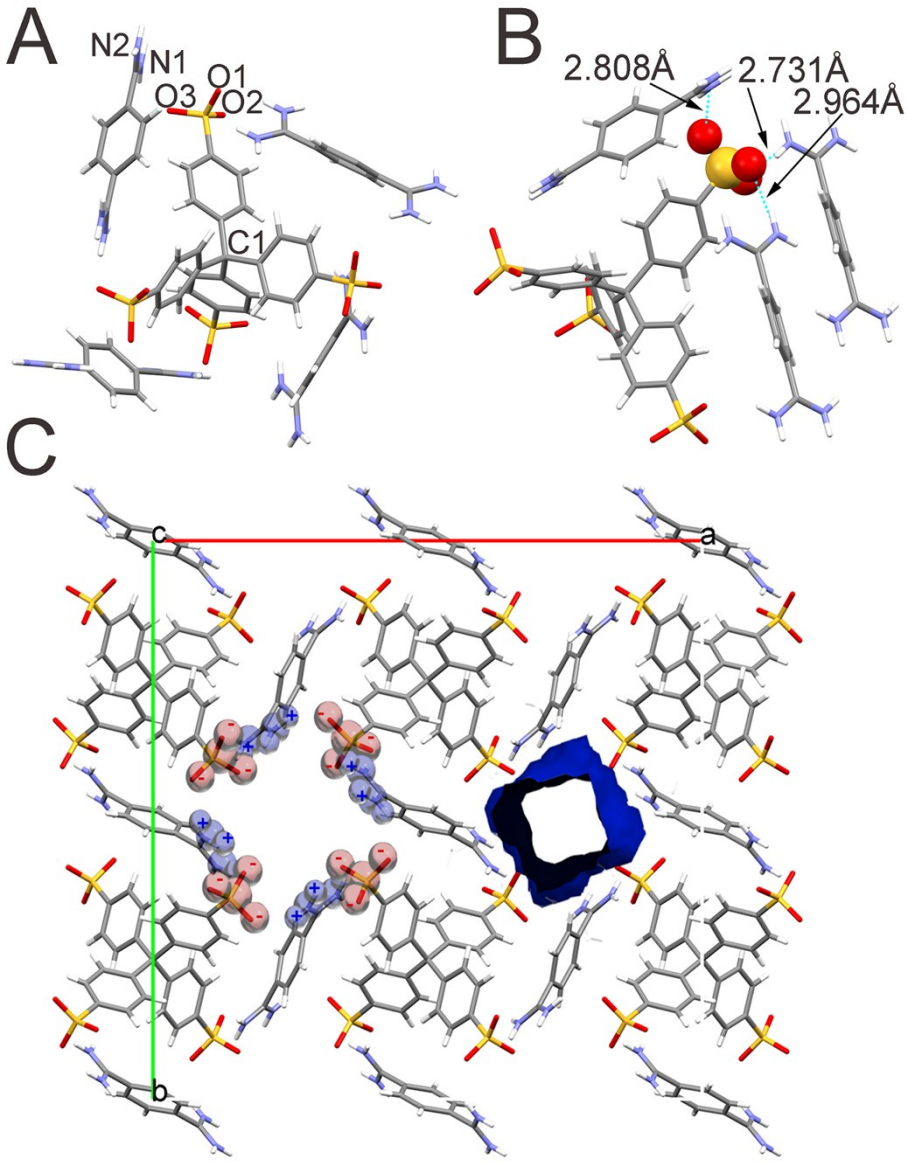

Figure S6. A) Portion of the CPOS-5 crystal structure collected at 273 K. The crystal structure is built on the electrostatic interactions between the anions TBS and cations DAB. B) Anions and cations are intimately connected by means of H-bonding. Four DAB molecules surround the anion, biting with H-bonding two sulphonate groups each (2.808 and 2.964 Å), while other four DAB molecules link through H-bonding (2.731 Å) two sulphonate groups belonging to two different TBS anions, building the 3D structure. C) The projection of CPOS-5 along *c*-axes: the negative and positive charges of synthons lining the channel walls are highlighted.

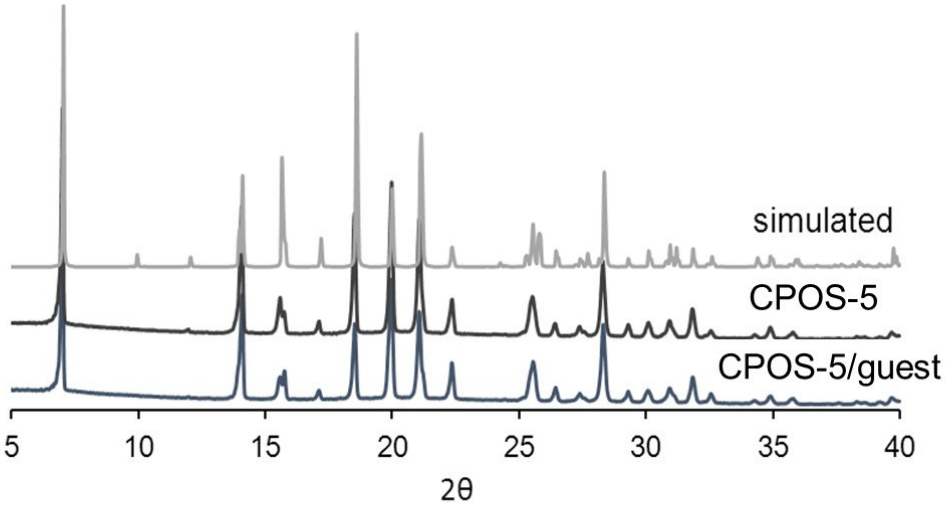

Figure S7. Experimental PXRD patterns of CPOS-5 and CPOS-5 with guests compared with the simulated pattern (from SC-XRD collected at 273 K).

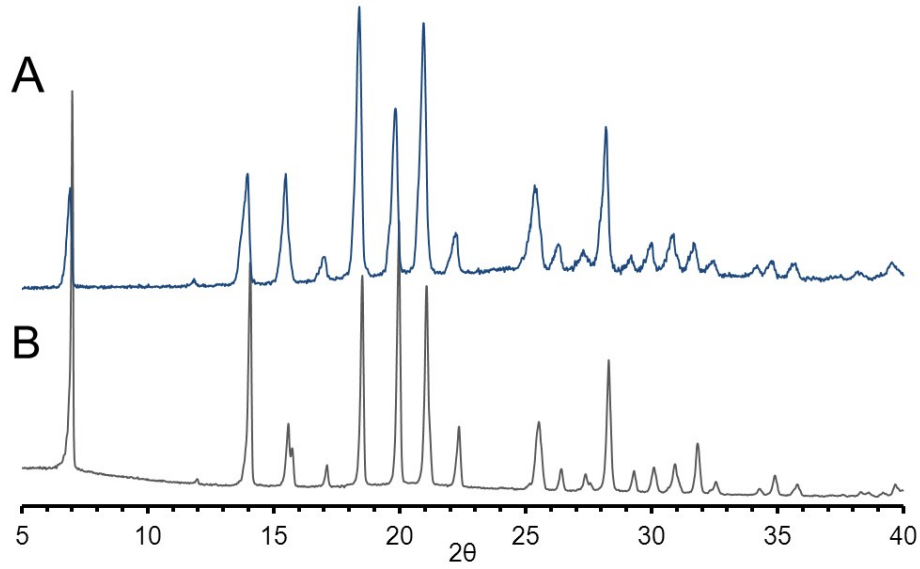

Figure S8. Experimental PXRD patterns of CPOS-5 (A) after water soaking for 24 hours at room temperature (A) and of the empty CPOS-5 compound (B).

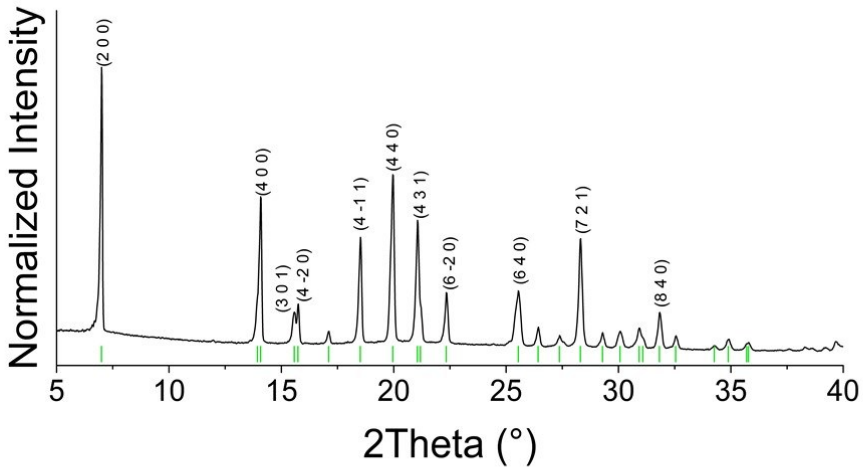

Figure S9. Indexing of PXRD pattern of CPOS-5. Indexing was performed using the TOPAS-Academic-64 V6 software package.

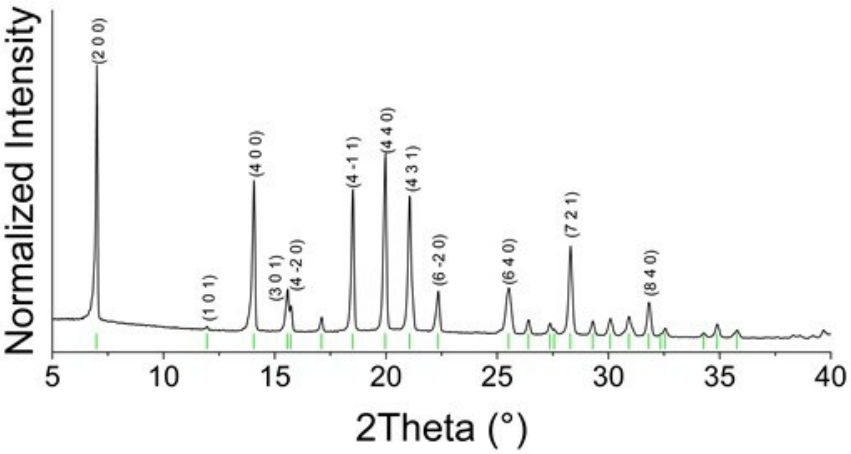

Figure S10. Indexing of PXRD pattern of activated CPOS-5. Indexing was performed using the TOPAS-Academic-64 V6 software package.

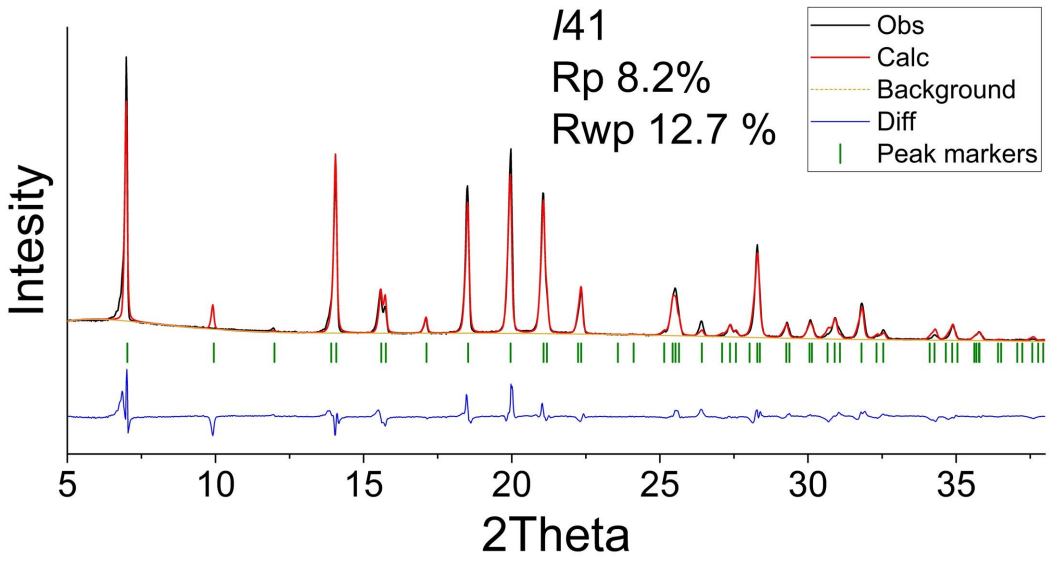

Figure S11. Rietveld refinement pattern of powder X-ray data for empty CPOS-5 using the TOPAS-Academic-64 V6 software package. The *hkl* indices are indicated as green markers and the difference plot are shown below. The black and red lines represent the observed and calculated traces, respectively, while the dotted yellow line represents the background plot.

Table S2. Crystallographic data for the PXRD Rietveld refinement of empty CPOS-5.

Identification code	**Empty CPOS-5**
Empirical formula	$C_{20.25}H_{20}N_4O_6S_2$
Formula weight	479.54
Temperature/K	N/A
Crystal system	tetragonal
Space group	$I4_1$
a/Å	25.1436
b/Å	25.1436
c/Å	7.7155
α/°	90
β/°	90
γ/°	90
Volume/Å^3	4877.74
Z	8
ρ_{calc}g/cm^3	1.3059
Rp	8.2 %
Rwp	12.7 %

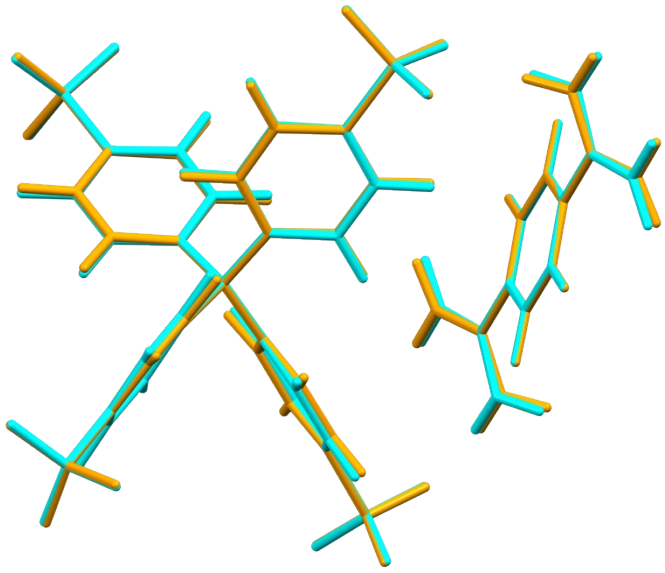

Figure S12. An overlay for the final DFT optimized (orange) and PXRD refined (cyan) structures of CPOS-5. The RMS difference between the structures is 0.999. The overlay picture was created using the Mercury V 3.9 software.

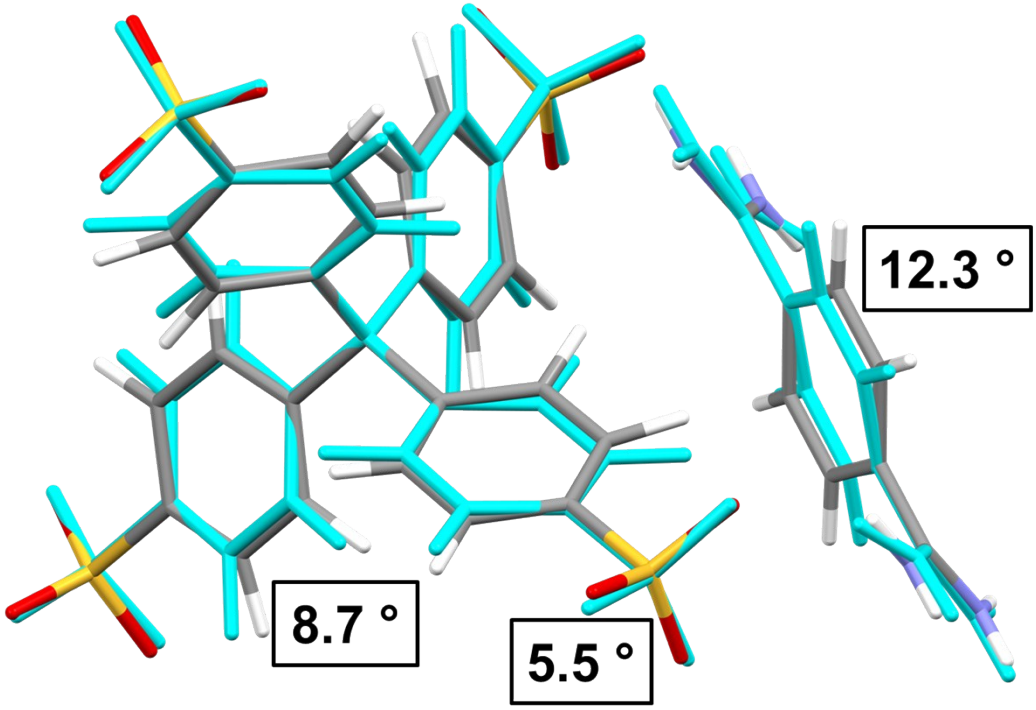

Figure S13. An overlay for the final PXRD Rietveld refined structure (cyan) of empty CPOS-5 at room temperature and the 273 K SCXRD structure of CPOS-5 (colored by element). The changes in tilt angle for the TBS phenyl rings, sulfonate group and DAB phenyl rings are indicated. The overlay was performed using the Mercury V 3.9 software.

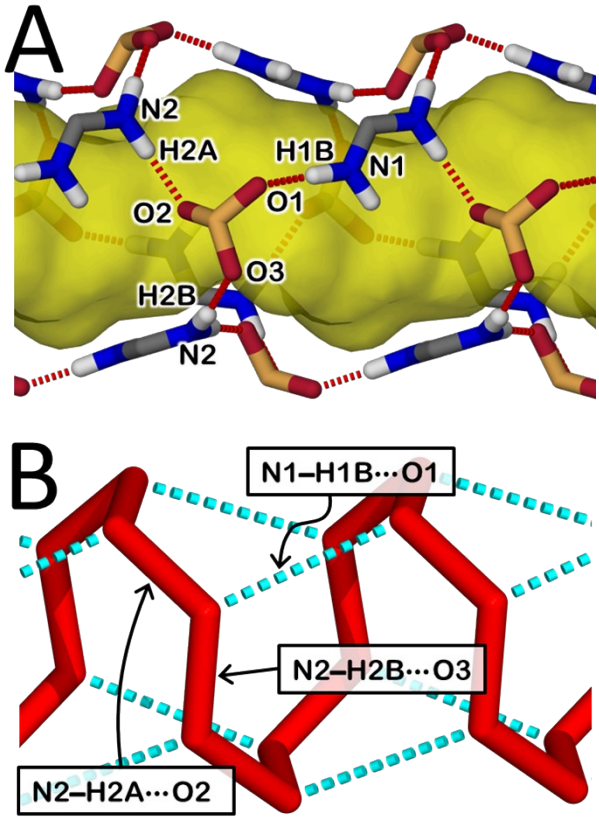

Figure S14. A) The amidinium and sulfonate moieties of CPOS-5 shown in stick representation with the H-bond indicated as a dotted red line and the relevant atoms for the H-bonds indicated. B) A schematic of the hydrogen bonded spiral form by the sulfonate and amidinium moieties with the unique H-bonds indicated.

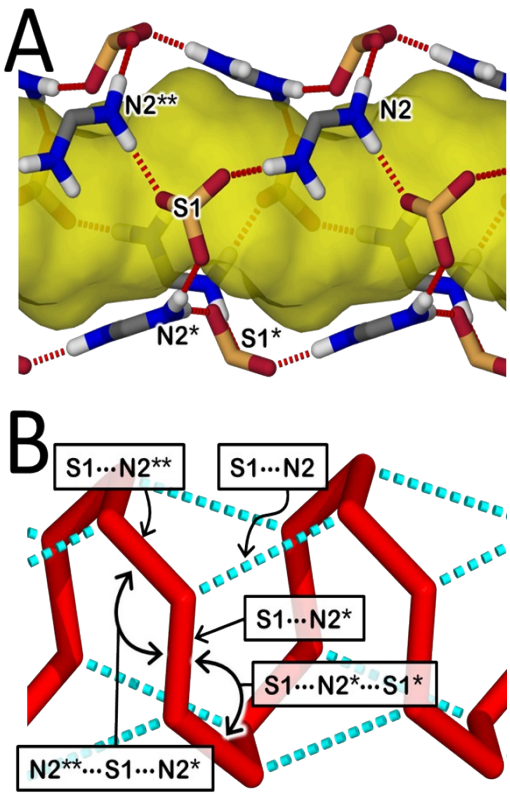

Figure S15. A) The amidinium and sulfonate moieties shown in stick representation with the H-bond indicated as a dotted red line and the relevant atoms for the schematic spiral measurements indicated. B) A schematic drawing of the hydrogen bonded network formed by the sulfonate and amidinium moieties with the relevant distances and angles forming the helix indicated by red lines.

Table S3. Selected distances and angles of amidinium and sulfonate hydrogen bonds forming the helical pattern for CPOS-5 crystal structure (SCXRD) at 273 K and the DFT/Rietveld determined for empty CPOS-5 structure (PXRD) at room temperature. The atoms associated with the measurements are shown in the figures reported above.

	D···A distance (Å)		Δ distance (Å)	D–H···A angle (°)		Δ angle (°)
	CPOS-5	**Empty CPOS-5**		**CPOS-5**	**Empty CPOS-5**	
	SCXRD	PXRD		SCXRD	PXRD	
N2–H2A···O2	2.9509(2)	3.015	0.064	171	174	3
N2*–H2B···O3	2.8063(2)	2.945	0.139	166	160	-6
N1–H1B···O1	2.7318(2)	2.759	0.027	142	174	32

Footnote: Symmetry equivalence atoms – N2* $\left(y-\frac{1}{4}, \frac{3}{4}-x, \frac{3}{4}+z\right)$

Table S4. Selected distances of amidinium and sulfonate hydrogen bonds forming the helical pattern for CPOS-5 crystal structure (SCXRD) at 273 K and the DFT/Rietveld determined for empty CPOS-5 structure (PXRD) at room temperature. The atoms associated with the measurements are shown in the figures reported above.

	CPOS-5	**Empty CPOS-5**	**Δ**
S1···N2* (Å)	3.643	3.713	0.07
S1···N2** (Å)	3.762	3.731	-0.031
S1···N2 (Å)	6.094	6.172	0.078
N2**···S1···N2* (°)	109	114	5
S1···N2*···S1* (°)	127	125	-2

5. Gas Adsorption Measurements

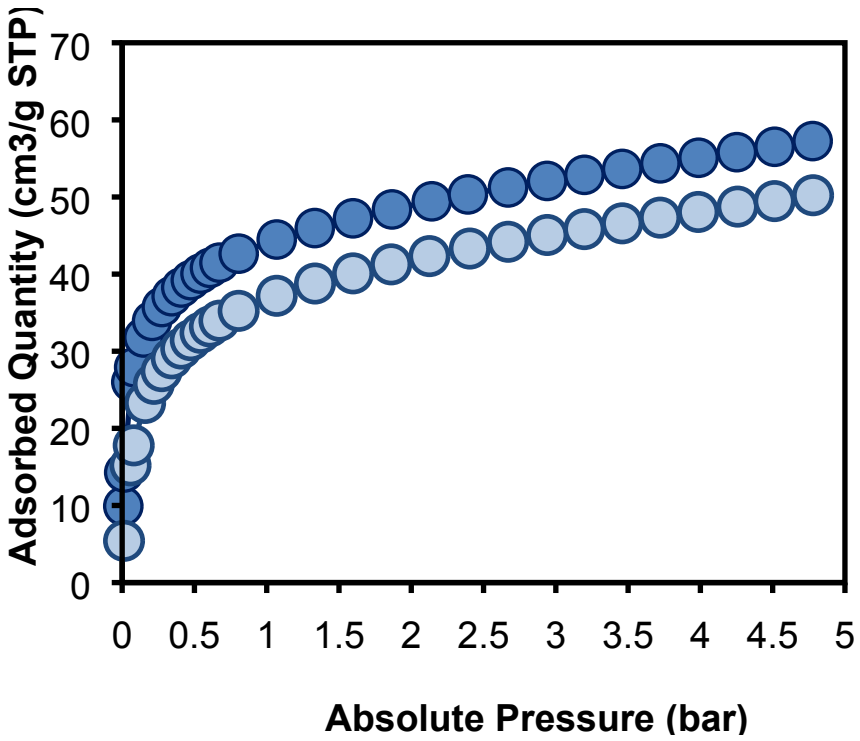

Figure S16. CO_2 adsorption isotherms of empty CPOS-5 at 273 K (dark blue) and 298 K (bright blue) up to 5 bar.

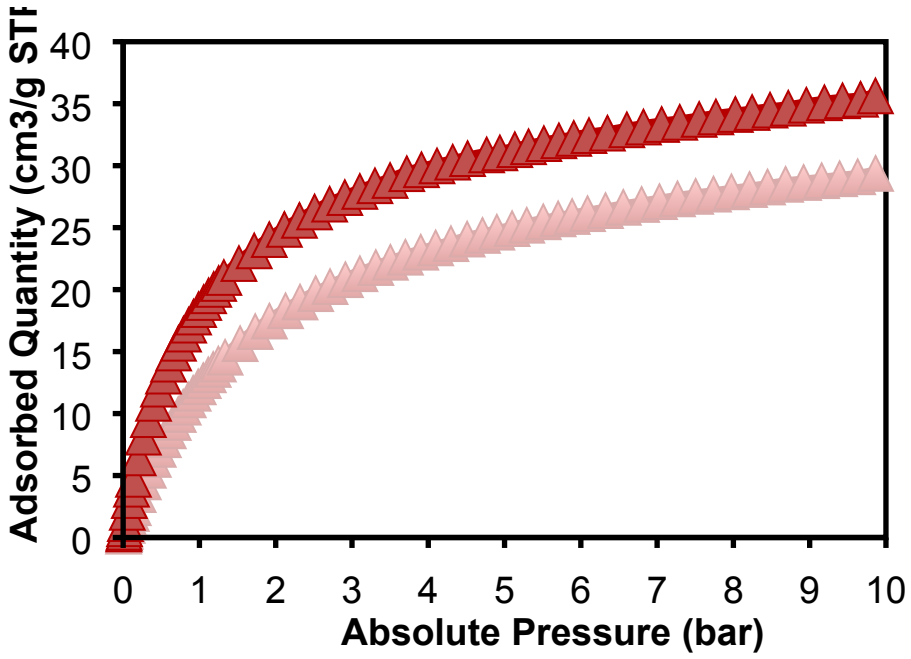

Figure S17. CH_4 adsorption isotherms of empty CPOS-5 at 273 K (dark red) and 298 K (bright red) up to 10 bar.

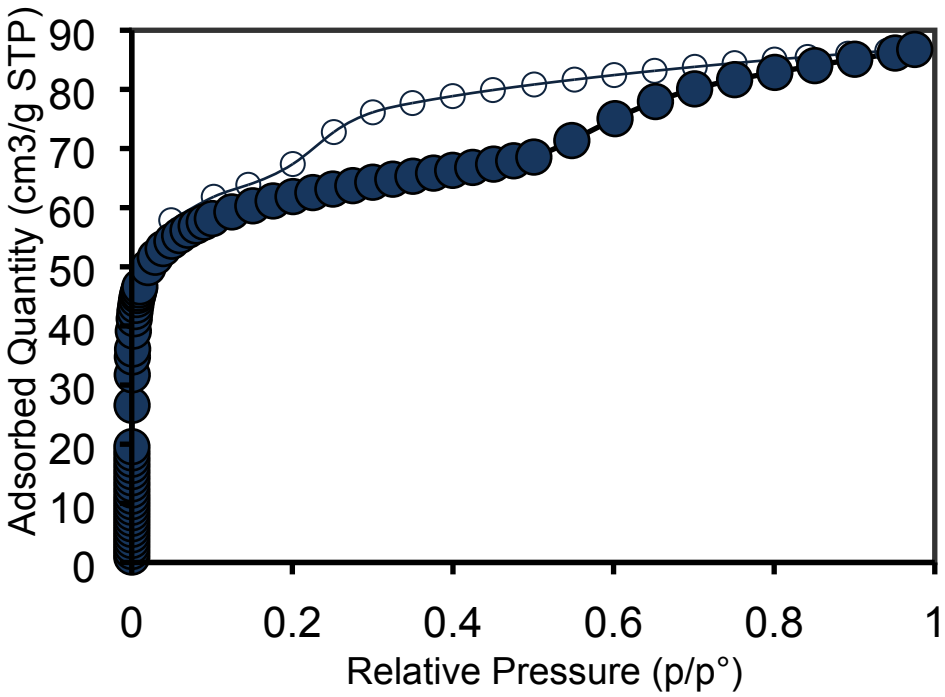

Figure S18. CO_2 adsorption/desorption isotherms of CPOS-5 at 195 K

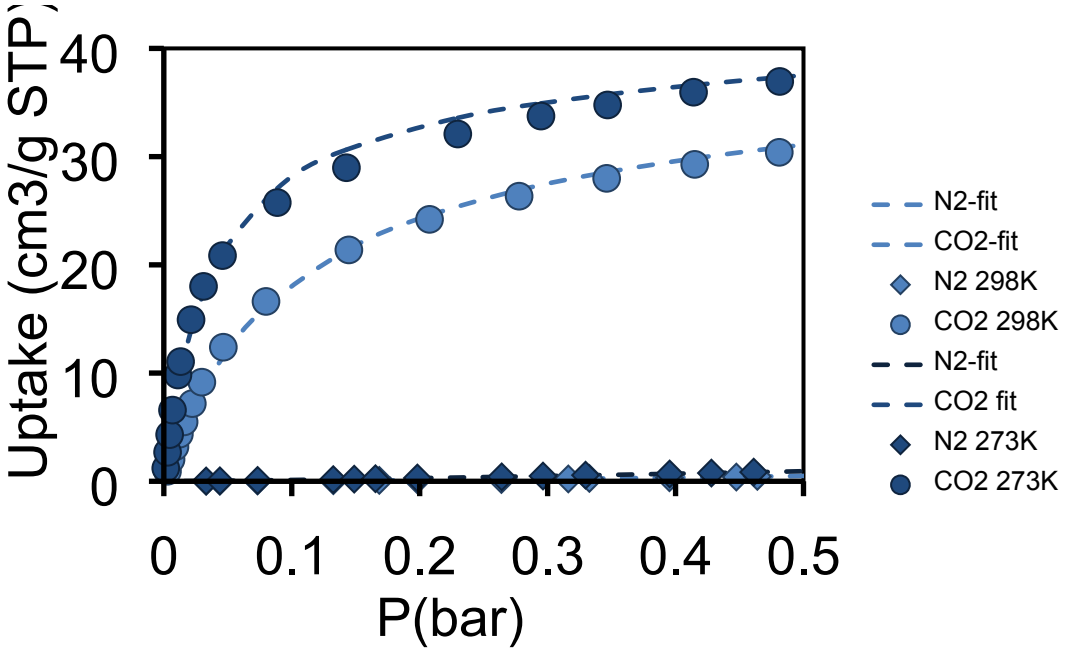

Figure S19. Experimental (full dots) and fitted (dashed line) CO_2 isotherms collected at 273 K(dark blue) and 298 K (light blue) of empty CPOS-5 compared to experimental (full rhombus) and fitted (dashed line) N_2 isotherms collected at 273 K (dark blue) and 298 K (light blue).

Table S5. Parameters from the nonlinear least square fit of CO_2 and N_2 adsorption isotherms.

	CO_2	**CO_2**	**N_2**	**N_2**
	273 K	**298 K**	**273 K**	**298 K**
	dual site Langmuir	*dual site Langmuir*	*Langmuir Freundlich*	*Langmuir Freundlich*
K_A	0.078 bar^{-1}	88.03 cm^3/g		
M_A	67.14 cm^3/g	88.03 cm^3/g		
K_B	24.44 bar^{-1}	10.44 bar^{-1}		
M_B	37.53 cm^3/g	34.72 cm^3/g		
K			0.0076 bar^{-1}	0.0030 bar^{-1}
M			1086.8 cm^3/g	29491.1 cm^3/g
t			1.27	1.70

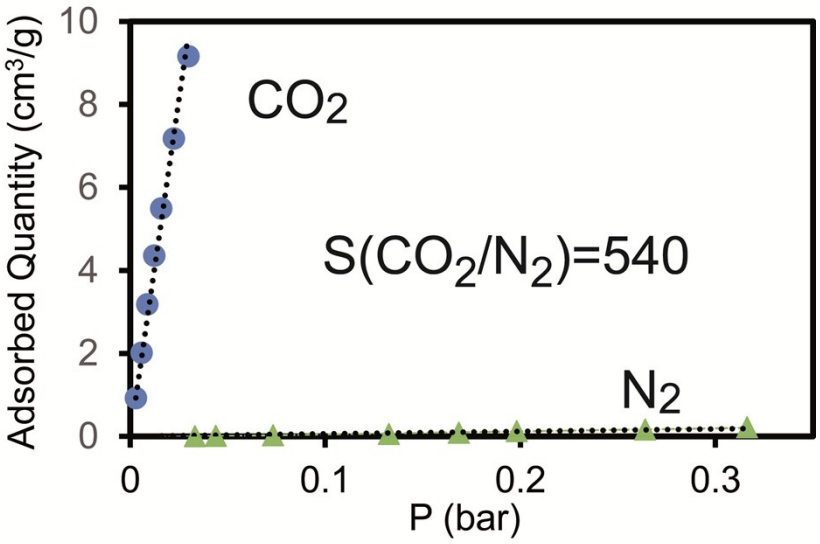

Figure S20. CO_2 and N_2 adsorption isotherms at low pressures and room temperature for the determination of the CO_2/N_2 adsorption selectivity, as calculated from the ratio of the Henry's constants. The CO_2/N_2 selectivity is of 540.

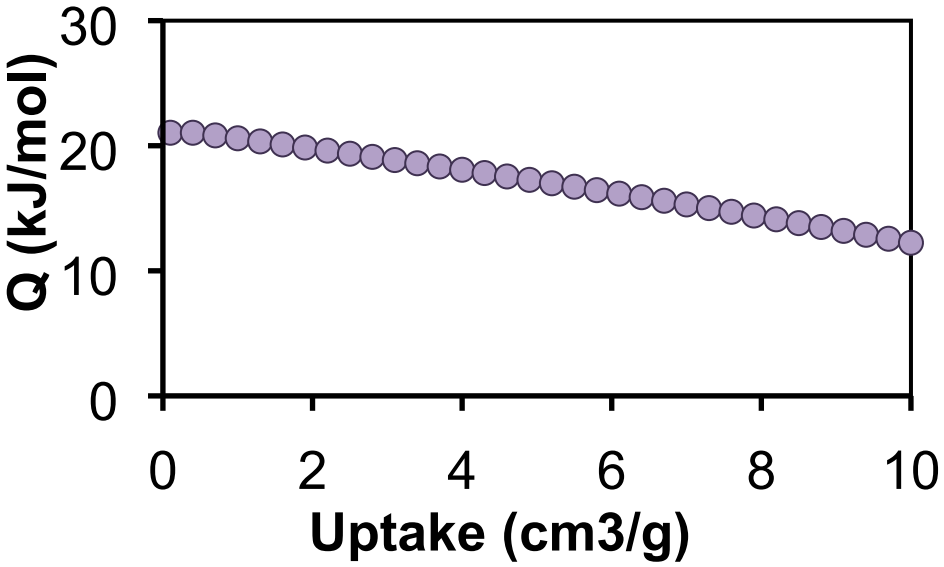

Figure S21. Methane isosteric heat of adsorption calculated on 298 K and 273 K adsorption isotherms of CPOS-5. The CH_4 adsorption isotherms were fitted using a Langmuir equation. At 298 K, M = 34.09 cm^3/g, K=0.55 bar^{-1} and, at 273 K, M = 38.42 cm^3/g K=0.92 bar^{-1}.

6. Solid State NMR

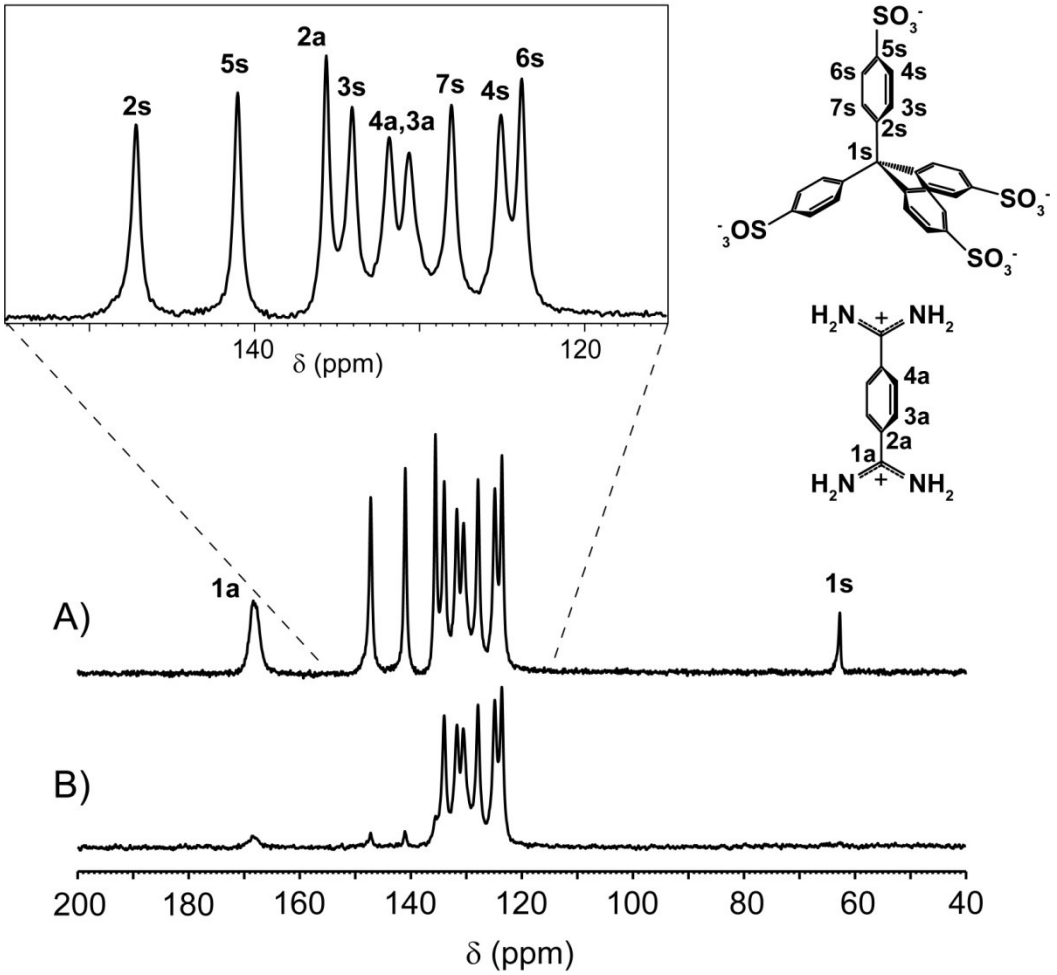

Figure S22. $^{13}C\{^{1}H\}$ CP MAS spectra of CPOS-5 collected at a spinning speed of 12.5 kHz and variable contact times: 2 ms (A) and 0.05 ms (B).

The NMR-WEBLAB software[6] was used to simulate the effects of motion on ^{13}C CSA shapes of CO_2 at different temperatures. The axially symmetric chemical shift tensors of δ_{11}/δ_{22}=232.8 ppm and δ_{33}=-82.5 ppm for CO_2 solid were taken as reported by A. Pines et al.[7] They were applied for the simulations taking into account the drift of the observed isotropic values at variable temperature. The isotropic chemical shift (δ_{iso}) of adsorbed CO_2 in CPOS-5 increases on lowering the temperature from 125.8 ppm up to 127.0 ppm owing to a stronger magnetic susceptibility effect. The simulation was performed using a 4-sites 90° jumps at an intermediate motion regime. The CO_2 inclination angle (θ) varies between 56.8° and 58.1° depending upon temperature and loading. A Gaussian distribution of angles ($\sigma\theta$°) was used in the simulations.

Table S6. NMR Parameters as obtained from the simulation of the ^{13}C static NMR spectra of CPOS-5 under $^{13}CO_2$ atmosphere. $\delta_{11}/\delta_{22}/\delta_{33}$ correspond to the main components of the chemical shift tensors, δ_{iso} isotropic chemical shift, *k* (Hz) rotational rates, θ (°) CO_2 inclination angles. The percentage (%) of CO_2 in CPOS-5 was estimated from the area of the deconvoluted peaks in the ^{13}C static NMR spectra.

T (K)	δ_{iso} (ppm)	δ_{11}/δ_{22} (ppm)	δ_{33} (ppm)	k (Hz)	θ (°)	σθ (°)	CO_2 per unit cell	% CO_2 in CPOS-5
295	125.8	237.45	-97.5	$7\ 10^6$	56.8	0.4	5.9	89.6
273	126.0	237.65	-97.3	$3\ 10^6$	57.5	0.8	6.2	94.6
260	126.2	237.85	-97.1	$1\ 10^6$	57.6	0.8	6.3	96.5
245	126.4	238.05	-96.9	$8\ 10^5$	57.8	1.0	6.4	97.7
230	126.8	238.45	-96.5	$5\ 10^5$	58.0	1.5	6.4	98.3
215	127.0	238.65	-96.3	$4\ 10^5$	58.1	1.8	6.5	99.5

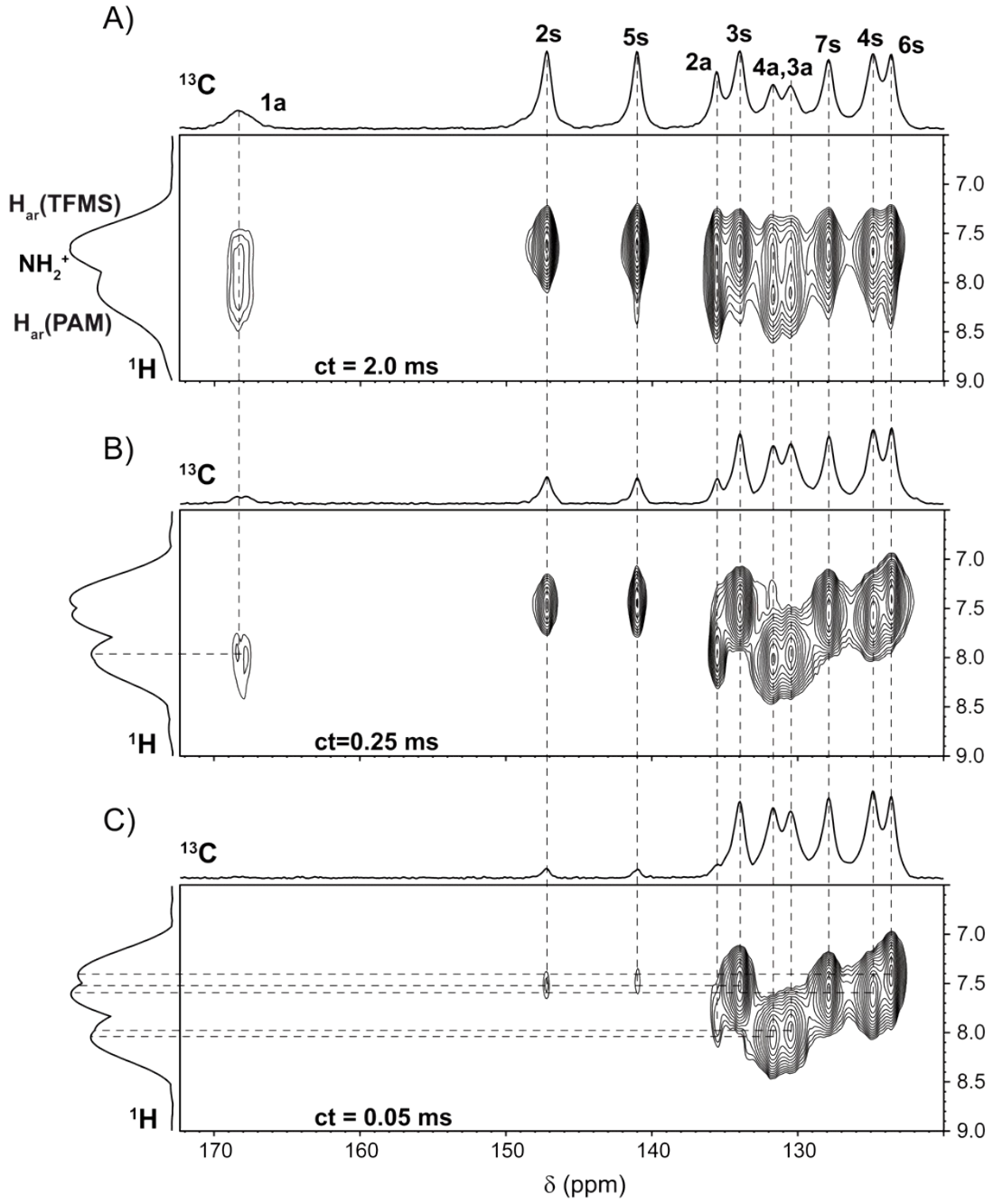

Figure S23. 2D ^{1}H-^{13}C PMLG HETCOR NMR spectra of CPOS-5 collected at a spinning speed of 12.5 kHz and variable contact times: 2 ms (A), 0.25 ms (B) and 0.05 ms (C).

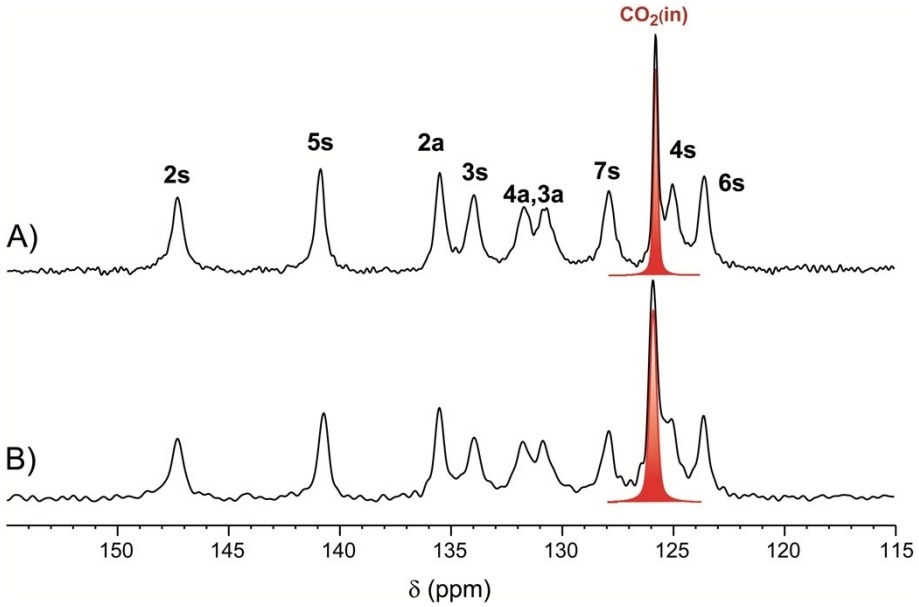

Figure S24. $^{13}C\{^{1}H\}$ CP MAS spectra of CPOS-5 in the presence of $^{13}CO_2$ collected at a spinning speed of 8 kHz and 5 ms of contact time at 296 K (A) and at 266 K (B).

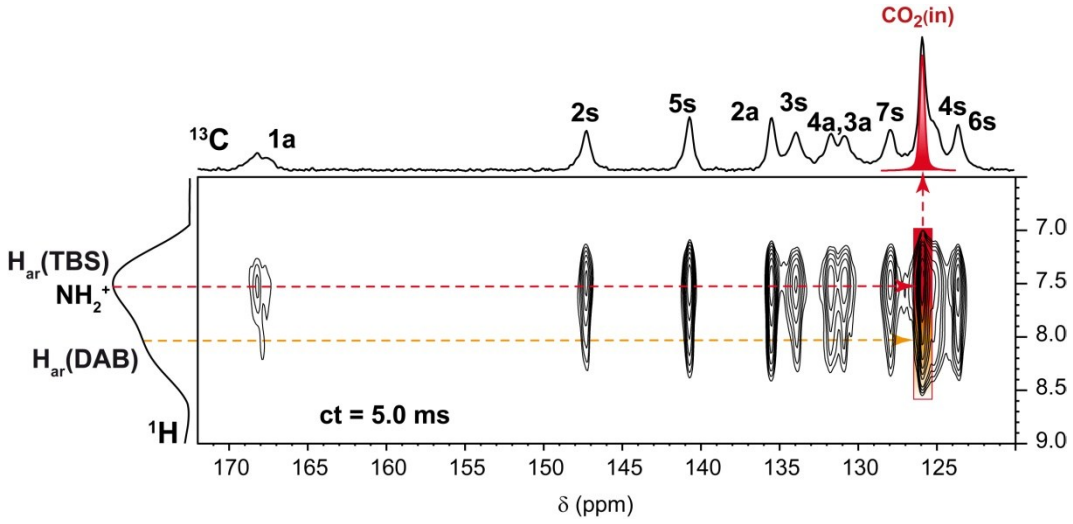

Figure S25. 2D ^{1}H-^{13}C PMLG HETCOR NMR spectrum of CPOS-5 in the presence of $^{13}CO_2$ collected at 266 K, at a spinning speed of 8 kHz and at 5 ms of contact time.

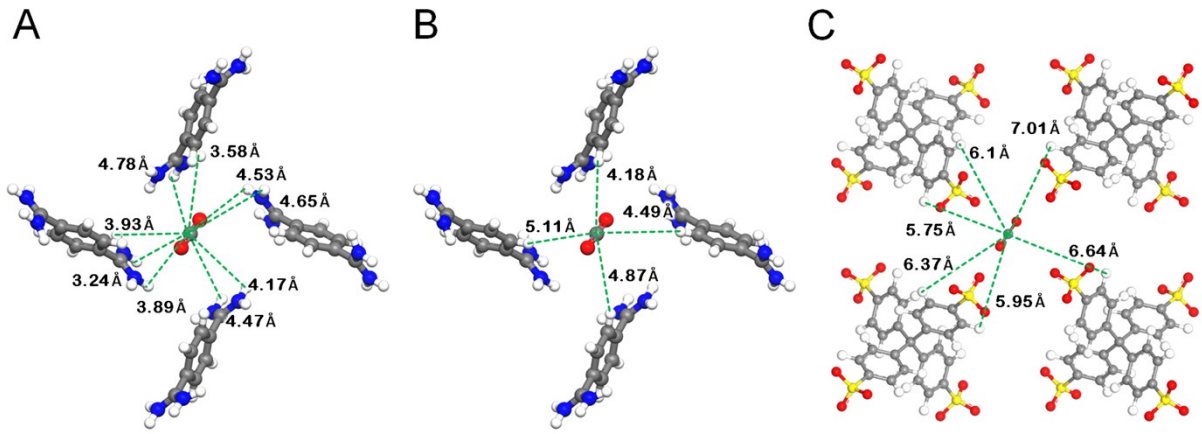

Figure S26. Intermolecular distances (less than 7 Å) for the 1 CO_2 molecules per channel modelled by DFT calculations (see Computational data) between NH_{DAB}---C_{CO2} (A); CH_{DAB}---CO_2 (B); CH_{TBS}---C_{CO2} (C).

7. Computational data

The atoms in the frameworks were optimized as part of a periodic system using the CASTEP module of the Materials Studio software suite.[8] MM and MD calculations were performed using the Forcite-Plus module. Single point energies were used to determine the interaction energies and were calculated as follows:

$E(host\ +\ guest)$: *The full crystal structure with the guest molecules included.*

$E(host)$: *The guest molecules are removed from the periodic model.*

$E(guest)$: *The host molecules are removed from the periodic model.*

$E_{int}(host\ -\ guest)$: *The host – guest interaction energy*.

$E_{int}(guest\ -\ guest)$: *The guest – guest interaction energy*.

$$E_{int}(host - guest) = E(host\ +\ guest) - (E(host)\ +\ E(guest))$$

$$E_{int}(guest - guest) = E(guest\ A\ and\ B) - (E(guest\ A) + E(guest\ B) + \cdots)$$

Table S7. Forcite energy parameters.

Quality	Fine
Force field	pcff
Charges	Current (obtained from CASTEP)
Summation method	
Electrostatic	Group based
van der Waals	Group based
Ewald accuracy	1.0e-5 kcal/mol

Table S8. Forcite Geometry optimization parameters.

Geometry optimization	
Algorithm	Quasi-Newton
Energy tolerance	1.0e-4 kcal/mol
Force	0.005 kcal/mol/Å
Max iterations	750

Table S9. Forcite Quench Dynamics parameters.

Ensemble	NVT (constant V and T)
Temperature	298 K
Time step	1 fs
Simulation time	100 ps
Thermostat	Velocity scale (2 K)
Quench	Every 1000 frames

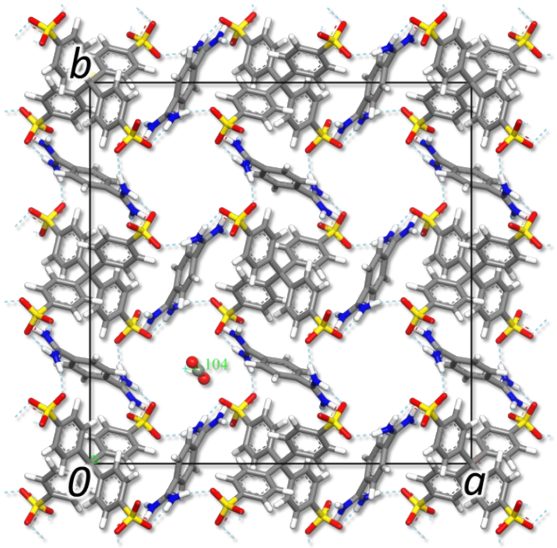

Figure S27. The computational model of the crystal structure used to scan a channel by moving a CO_2 molecule along the channel. The translation was achieved by placing a distance restraint between the CO_2 carbon and an anchor position within the channel and then changing the harmonic minimum distance of the restraint. This allows for optimization towards each newly set harmonic minimum distance and thus moves the CO_2 along the channel.

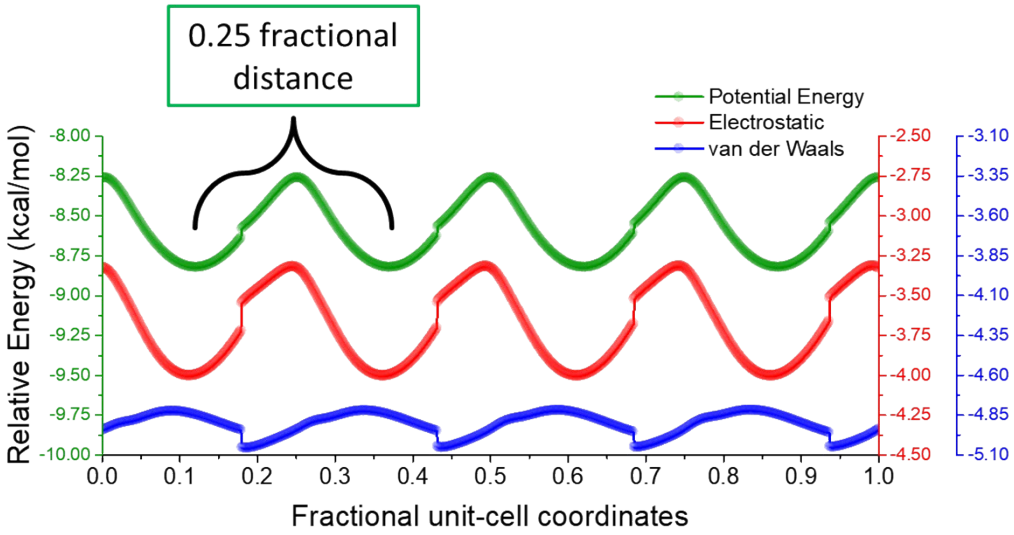

Figure S28. The results of the Molecular Mechanics scan for a CO_2 molecule moving along the channel. The simulation was performed without imposing symmetry element constraints (*P*1 space group) and the CO_2 minima positions are related by a 4_1 screw axis which conforms to the symmetry of host. Thus, from one minimum to the next a translation of 0.25 (fractional) along the *c*-axis and a rotation of 90° occur.

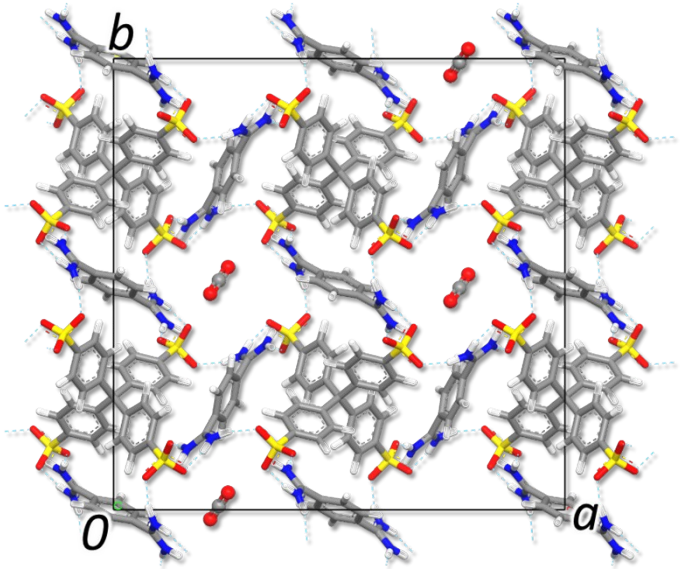

Figure S29. The computational model of the crystal structure used for the 1 CO_2 per channel in the unit cell (4 CO_2 molecules per unit cell MPU) by DFT optimization. The initial position of the CO_2 molecules was taken from the Molecular Mechanics scan of the host channel. The *P*2/*b* space group was used to speed up the calculation as well as maintain 1 CO_2 molecule per channel.

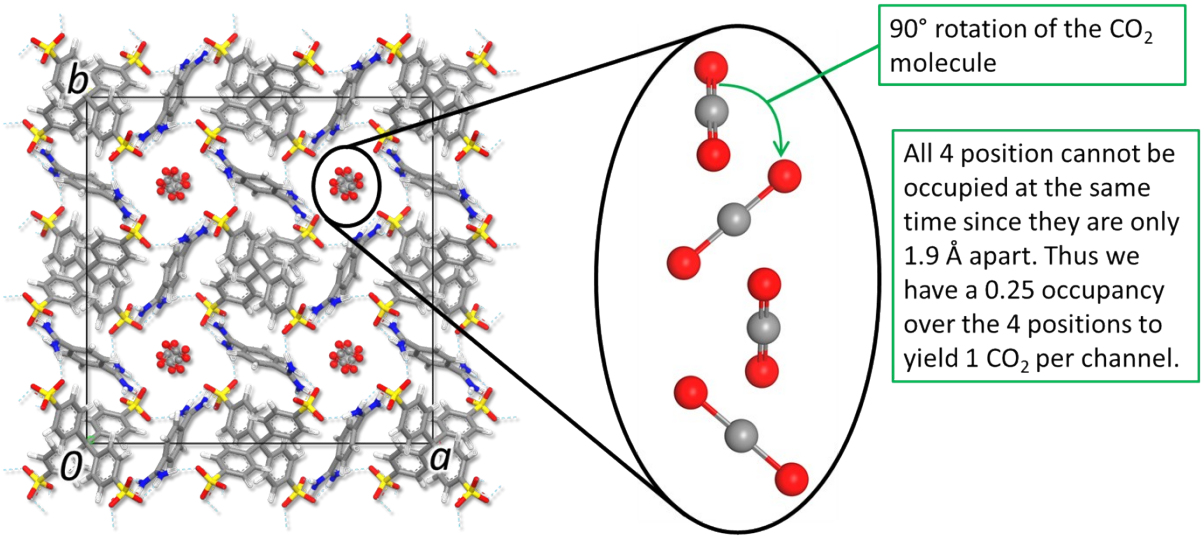

Figure S30. The DFT optimized CO_2 position, taken from the 1 CO_2 per channel model, with the host symmetry applied, highlighting the 90° rotation when the CO_2 moves from one site to the next along the *c*-axis.

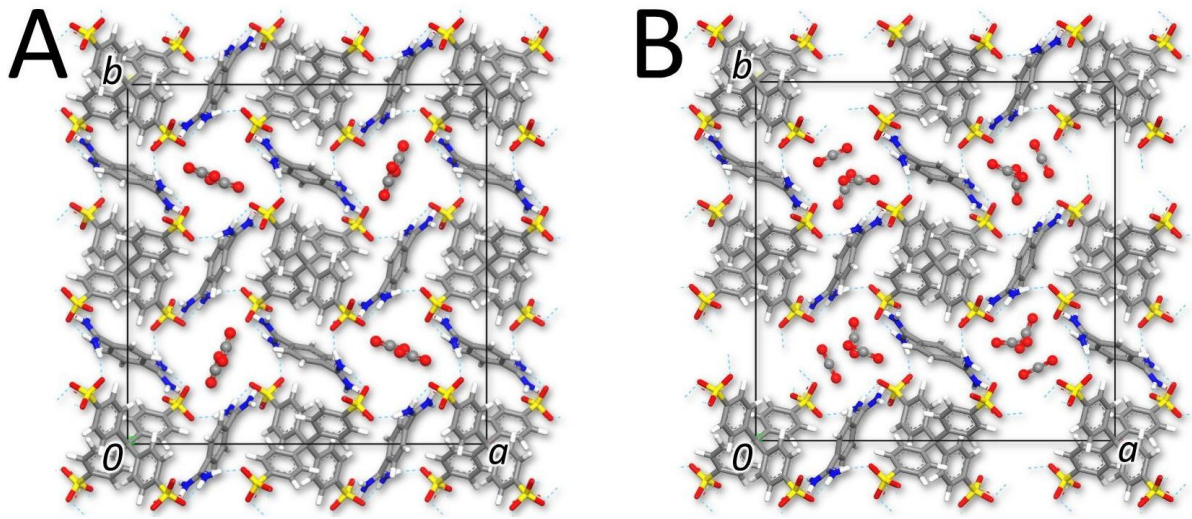

Figure S31. (A) The 2 CO_2 molecules per channel (8 CO_2 MPU) and (B) 3 CO_2 molecules per channel (12 MPU) from the computational model optimized by DFT calculations.

Table S10. The CO_2 angle between the main CO_2 axis and the crystallographic *c*-axis for the 1 CO_2, 2 CO_2 and 3 CO_2 molecules per channel models. The systems were optimized by means of DFT calculations.

Unique CO_2 positions	**4 MPU**	**8 MPU**	**12 MPU**
	1 CO_2 per channel (isolated)	**2 CO_2 per channel**	**3 CO_2 per channel**
Position 1	**49.2°**	**53.1°**	**68.0°**
Position 2		**60.2°**	**73.4°**
Position 3			**76.9°**

Table S11. Host--CO_2 and CO_2--CO_2 interaction energies for the 1 CO_2 and 2 CO_2 molecules per channel models as determined by DFT calculations.

Computational Model	Type of Interaction	Interaction energy (kcal/mol)	Interaction energy (kJ/mol)
1 CO_2 per channel (isolated, 4 MPU)	Host—CO_2	-8.08	-33.80
	Total E_{int} per CO_2 molecule	**-8.08**	**-33.80**
2 CO_2 per channel (8 MPU)	Host—1st CO_2	-8.30	-34.72
	Host—2nd CO_2	-7.04	-29.45
	CO_2—CO_2	-1.13	-4.74
	Total E_{int} per CO_2 molecule	**-8.03**	**-33.58**
3 CO_2 per channel (12 MPU)	Host—1st CO_2	-8.41	-35.18
	Host—2nd CO_2	-6.89	-28.82
	Host—3rd CO_2	-5.97	-24.98
	1st CO_2—2nd CO_2	-0.91	-3.79
	2nd CO_2—3rd CO_2	-1.03	-4.32
	3rd CO_2—1st CO_2	-0.90	-3.75
	Total E_{int} per CO_2 molecule	**-7.54**	**-31.55**

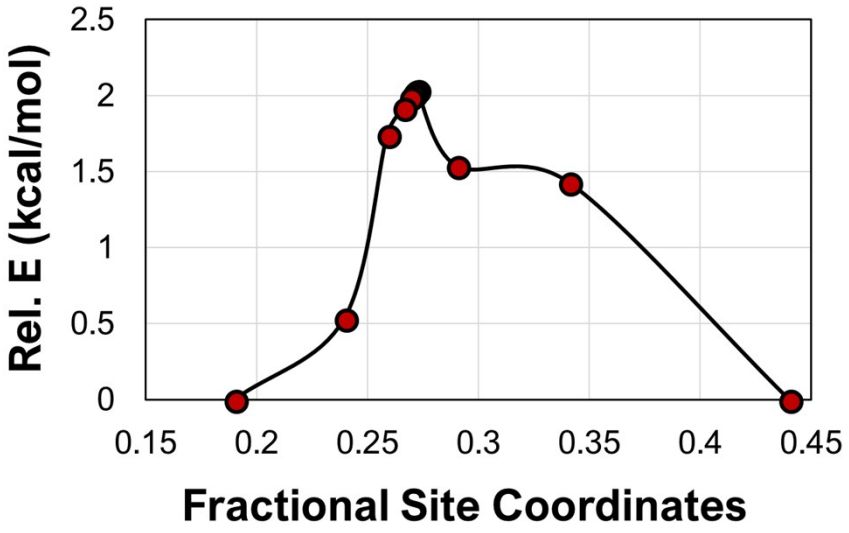

Figure S32. Energy barrier for 1 CO_2 molecule traveling from one site to the adjacent site along the channel using the DFT optimized CO_2 positions. The energy barrier is of 2.03 kcal/mol.

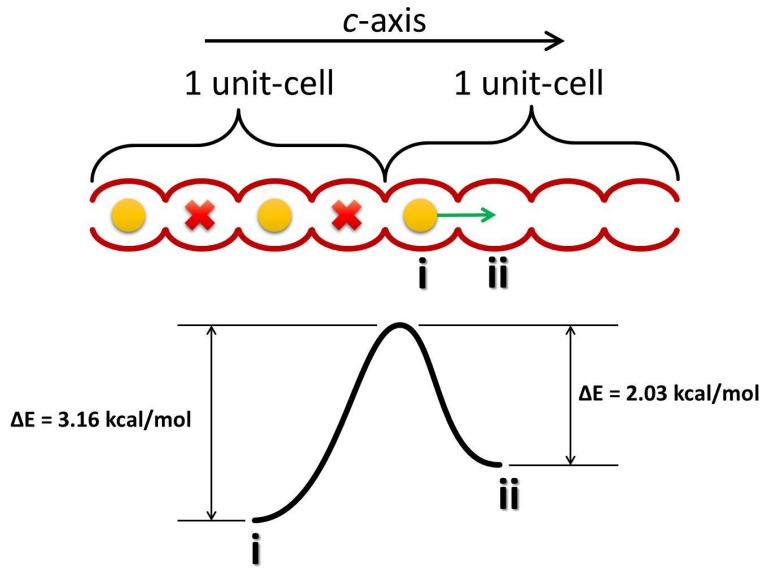

Figure S33. Energy barrier of CO_2 travelling along the channel when it interacts with another CO_2 molecule. The energy barrier is 3.16 kcal/mol owing to the CO_2--CO_2 interactions.

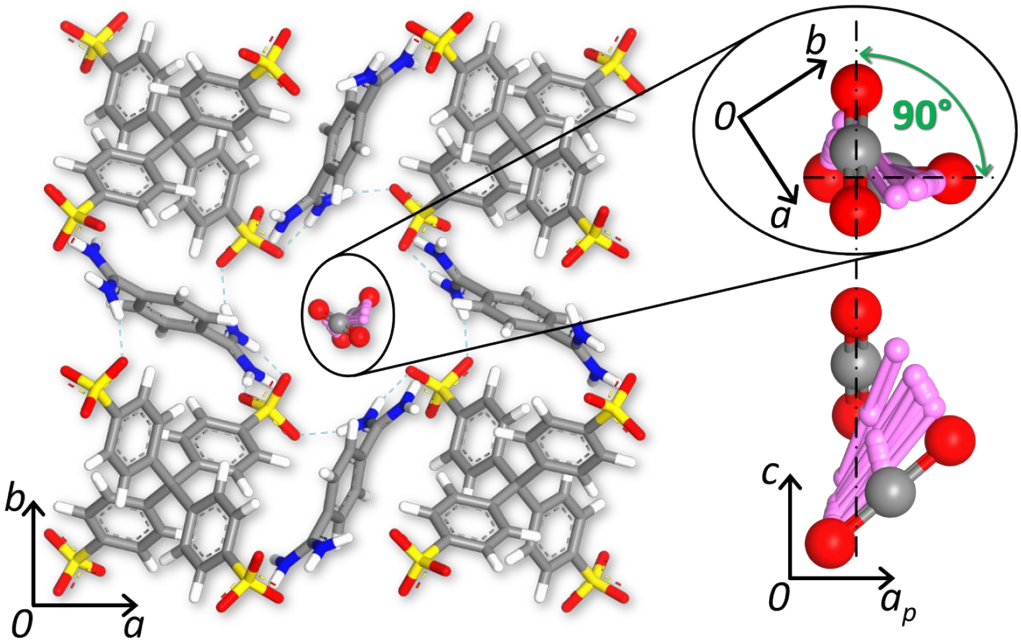

Figure S34. An overlay of all the CO_2 positions obtained from the transition state calculation by DFT method (1 CO_2 MPU). The CO_2 molecule travels from one site to the adjacent symmetry- related site along the channel axis (*c*-axis). The rotation angle of CO_2 projection onto the *ab*-plane changes by 90° as the molecules move from on site to the other. This corresponds to the screwing mechanism of CO_2 during the translational motion from one site to the next.

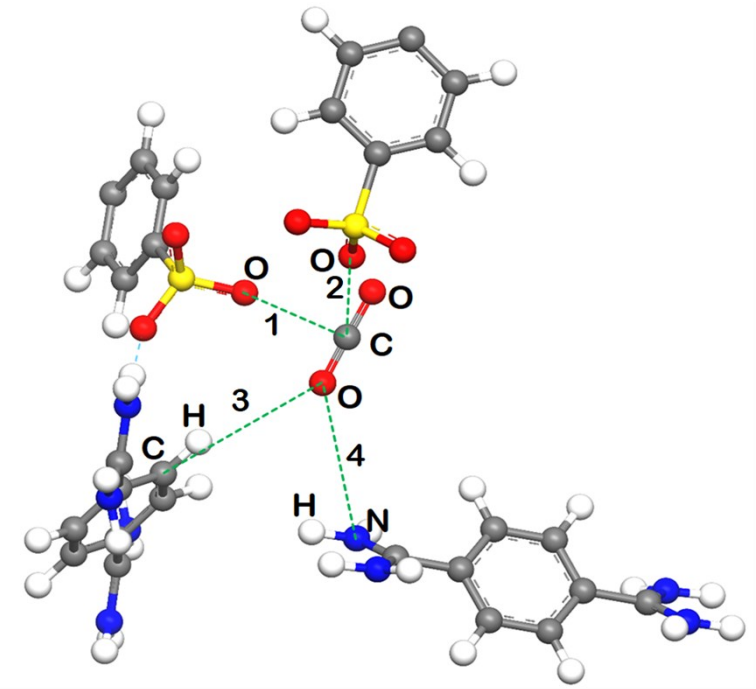

Figure S35. A visual of the main CO_2 host interactions as determined by means of the molecular electrostatic maps as calculated by DFT method (4 CO_2 MPU). The interactions have been labelled from 1 to 4 for the identification in the following Table listing the measurements.

Table S12. Selected CO_2 interaction distances and angles (in the case of H-bonds) for the DFT optimized CO_2 position for the model considering only one CO_2 per channel (of the unit cell). These interactions were selected based on the strongest electrostatic potentials obtain from the electrostatic potential maps. See Figure S34 for visual indication of these interactions.

	Interaction distance (Å)	**D···A distance (Å)**	**D–H···A angle (°)**
1 – O···C (Å)	2.825		
2 – O···C (Å)	3.428		
3 – C–H···O		4.308	162.1
4 – N–H···O		3.648	94.6

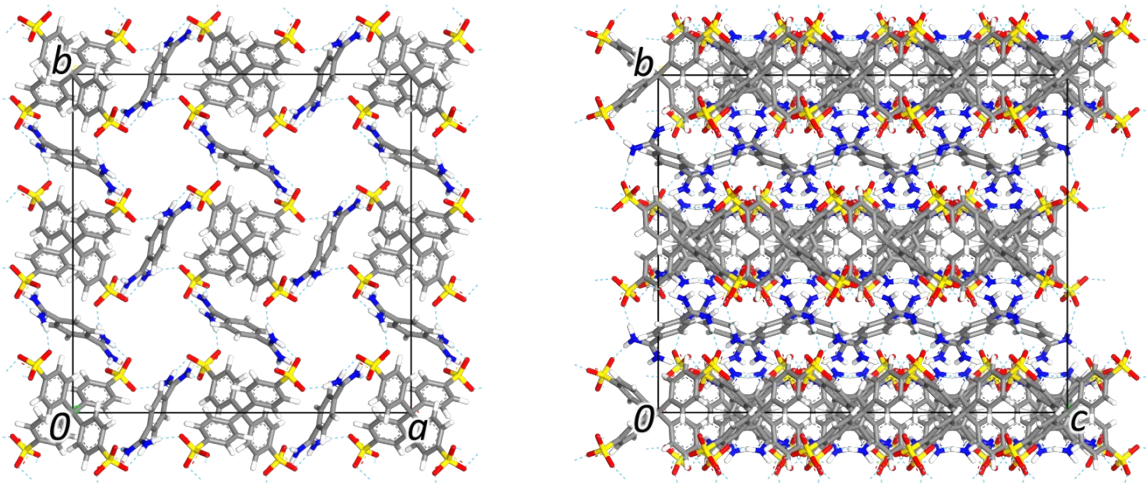

Figure S36. The computational model (super-cell consisting of 4 unit-cells along the *c*-axis) used for the molecular mechanics CO_2 loading simulations. Left – viewed along the *c*-axis. Right – viewed along the *a*-axis. The system is loaded 4 molecules at a time, one in each channel, to keep all the channels equivalent (1 CO_2 MPU).

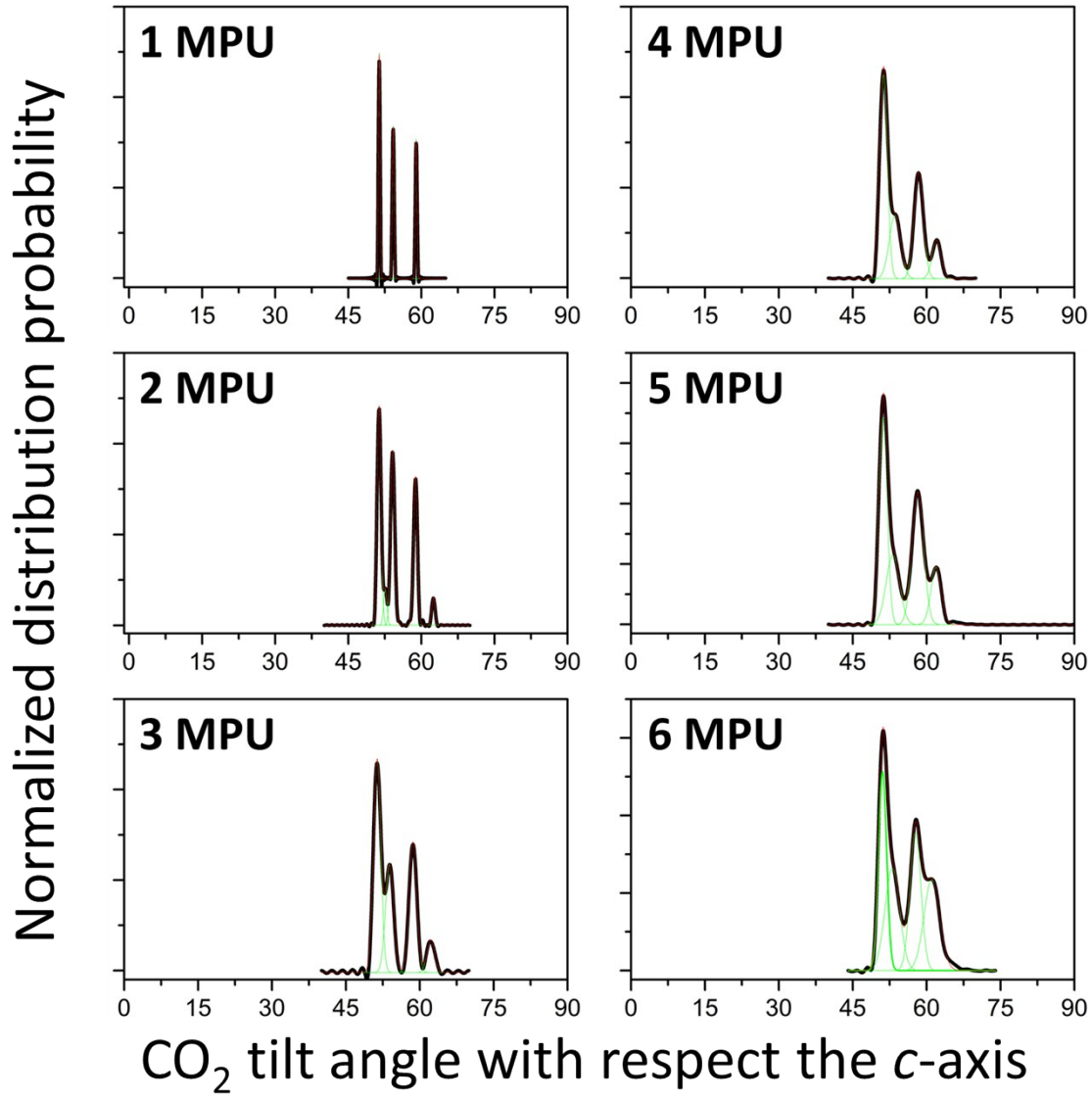

Figure S37. The CO_2 angle distribution for 1 – 6 MPU plotted against a normalized probability. The peak deconvolution is represented as green lines for each of the Gaussian peaks fitted to the data.

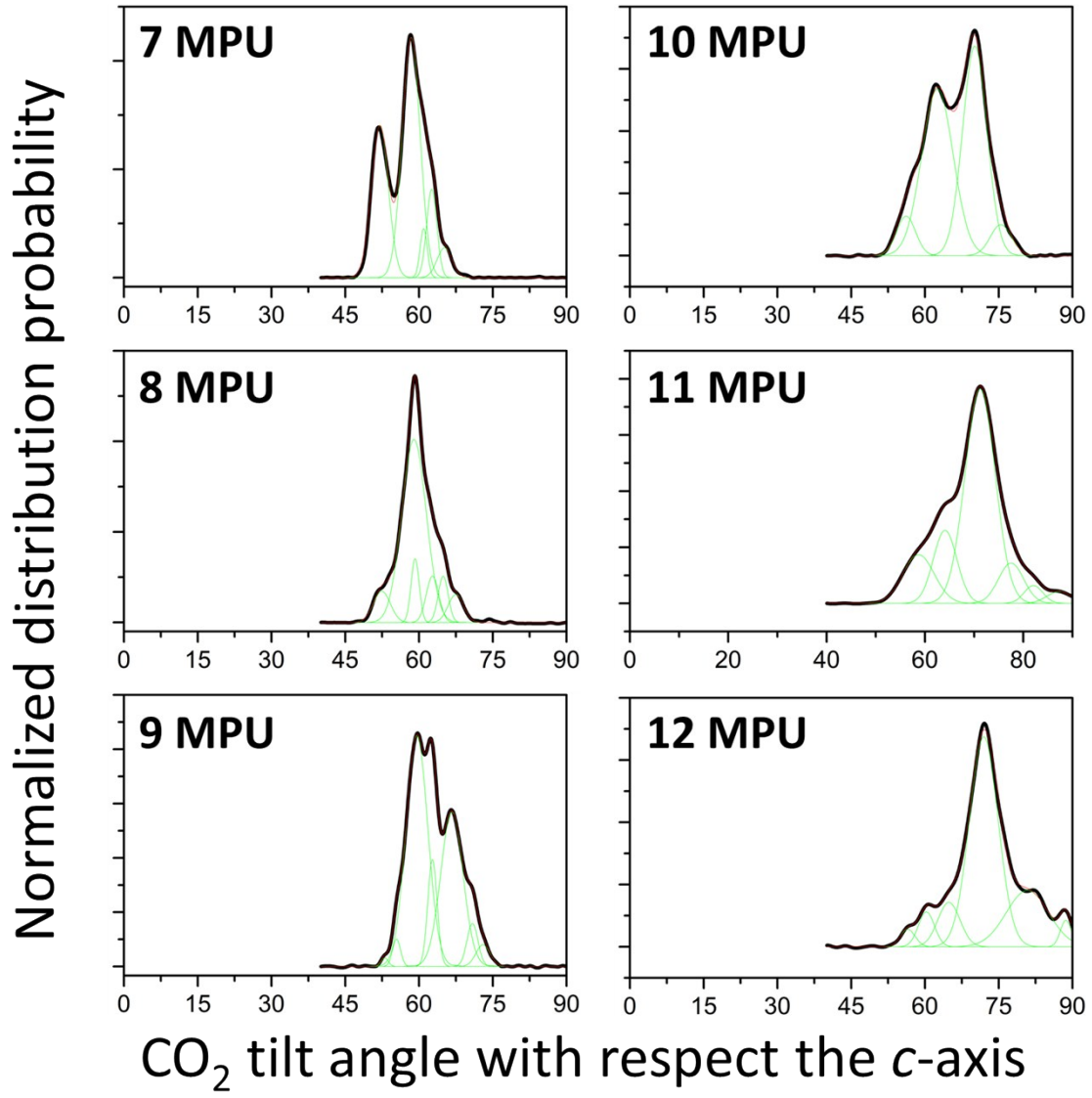

Figure S38. The CO_2 angle distribution for 7 – 12 MPU plotted against a normalized probability. The peak deconvolution is represented as green lines for each of the gaussian peaks fitted to the data.

Table S13. Comparison of CO_2 inclination angles (θ) at distinct pressure loadings, as determined by ^{13}C static NMR spectra and from theoretical calculations.

$^{13}CO_2$ loading in CPOS-5 (MPU)	**θ angle (°) From NMR**	**θ angle (°) From Theoretical model**	**Δ difference (°)**
5.98	56.8°	55.8°	1.0
6.32	57.5°	56.2°	1.3
6.51	57.6°	56.5°	1.1
6.54	57.8°	56.5°	1.3
6.55	58.0°	56.6°	1.4
6.63	58.1°	56.7°	1.4

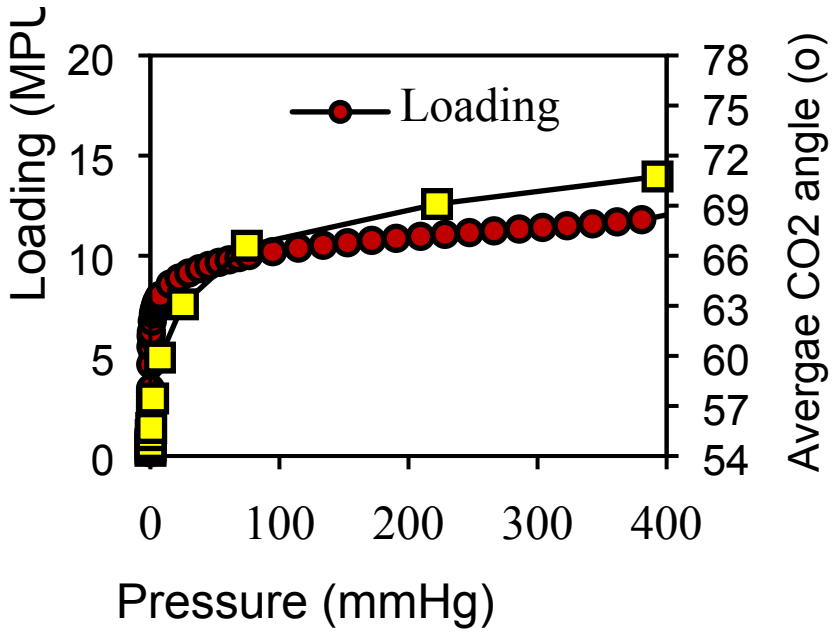

Figure S39. CO_2 adsorption isotherm at 195 K (red circles) compared to CO_2 inclination angles (θ) at distinct pressures as determined by theoretical calculations.

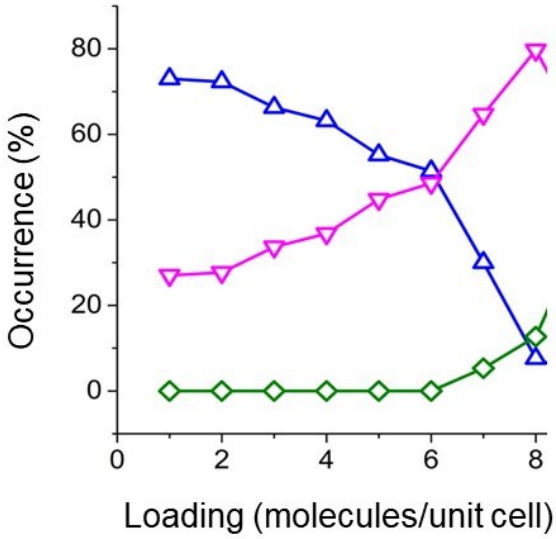

Figure S40. The percentage occurrence for each angle regime obtained from the deconvolution of the CO_2 angle distributions vs. loading in MPU. Each of the Gaussian peak is treated as an angle regime. The percentage occurrence vs. Loading in MPU is reported.

References

1 B. Sarmaa and A. Nangia, *Cryst. Eng. Comm.*, 2007, **9**, 628.

2 G. M. Sheldrick, *Acta Crystallogr., Sect. A*, 2015, **71**, 3.

3 O. V. Dolomanov, A. J. Blake, N. R. Champness and M. Schroder *J. Appl. Cryst*., 2003, **36**, 1283.

4 A. A. Coelho, *J. Appl. Cryst.*, 2003, **36**, 86.

5 C. F. Macrae, *et al. J. Appl. Cryst*., 2008, **41**, 466.

6 V. Macho, L. Brombacher, H. W. Spiess, H. W. *Appl. Magn. Reson.,* 2001, **20**, 405.

7 C. R. Bowers, H. W. Long, T. Pietrass, H. C. Gaede, A. Pines, *Chem. Phys. Lett.,* 1993, **205**, 168.

8 Materials Studio: Materials Studio Modeling Environment; Accelrys Software Inc.: San Diego, 2015.